




Journal Name

Crossmark

PAPER

RECEIVED
dd Month yyyyREVISED
dd Month yyyy

Characterising the role of final state interactions on neutrino energy estimation in the DUNE and Hyper-K era

Stephen Dolan^{1,*} , Jake McKean^{2,*}  and Laura Munteanu^{1,*} ¹CERN²Kyoto University, Department of Physics, Kyoto, Japan

*Authors to whom any correspondence should be addressed.

E-mail: stephen.joseph.dolan@cern.ch; mckean.jake.42u@st.kyoto-u.ac.jp; laura.munteanu@cern.ch**Abstract**

The Deep Underground Neutrino Experiment (DUNE) and Hyper-Kamiokande (Hyper-K) will measure neutrino oscillation parameters with an unprecedented precision that requires neutrino energy estimation to be controlled at the few-MeV level. A central challenge in achieving this is the modelling of the reinteractions of hadrons produced in neutrino-nucleus scatters with the residual nuclear medium, or final-state interactions (FSI). In this work we use state-of-the-art neutrino interaction event generators to review the impact of FSI modelling on the kinematic and calorimetric neutrino energy estimators used by Hyper-K and DUNE respectively, considering both the semi-classical intranuclear cascades (INCs) that dominate current simulations and a microscopic treatment based on a relativistic mean field calculation. We find that plausible variations of the FSI model introduce uncertainties on the neutrino energy estimation proxies that are at or above the precision on the energy scale control required for Hyper-K and DUNE projected neutrino oscillation sensitivities, highlighting the importance of careful FSI modelling to allow robust near detector constraints. We further demonstrate that the two experiments are sensitive to different aspects of the FSI models. Neutrino energy estimation at Hyper-K is most impacted by pion absorption and nuclear effects beyond the semi-classical paradigm, whilst the DUNE energy estimation is more affected by the modelling of how hadronic energy is shared between sources of visible and invisible energy in the detector. We discuss the implications of these findings for neutrino oscillation analyses and outline some of the key experimental and theoretical developments needed to bring FSI modelling uncertainties under control.

1 Introduction

The Deep Underground Neutrino Experiment (DUNE) [1, 2] and Hyper-Kamiokande (Hyper-K) [3, 4] long-baseline (LBL) neutrino oscillation experiments, due to start operation within the coming few years, represent a leap forward in prospects for precision measurements of neutrino oscillations. Aiming to increase the statistics for neutrino oscillation analyses by more than an order of magnitude with respect to the currently-operating T2K [5] and NOvA [6] LBL experiments, DUNE and Hyper-K are ideally placed: to make sub-percent level measurements of neutrino oscillation parameters; to probe CP violation in the lepton sector; to determine the neutrino mass ordering; and to search for physics beyond the three-flavour PMNS neutrino mixing paradigm [7, 8, 9, 10]. However, such precision will take neutrino oscillation measurements firmly out of the statistics limited era of current experiments into a regime where control over systematic uncertainties will underpin experimental success.

In general, LBL experiments operate by measuring the interactions of a predominantly muon neutrino beam twice: once at a near detector (ND) placed close to the neutrino beam production point, where oscillations are negligible, and again at a far detector (FD) placed downstream at a distance that approximately maximizes the neutrino oscillation probability. Experiments can operate using both neutrino and antineutrino enhanced beams. At the FD, experiments measure event rates (N_{FD}) of muon (μ) or electron (e) neutrino (ν) or antineutrino ($\bar{\nu}$) interactions that are sensitive to neutrino oscillation probabilities. Neglecting backgrounds and detector efficiency, these event rates can be written as:

$$N_{FD}^{\bar{\nu}_{\mu/e}} \propto P_{\bar{\nu}_{\mu} \rightarrow \bar{\nu}_{\mu/e}}^{osc} \Phi^{\bar{\nu}_{\mu}} \sigma^{\bar{\nu}_{\mu/e}}, \quad (1)$$

where P^{osc} is the oscillation probability for muon (anti)neutrinos oscillating into either electron or muon (anti)neutrinos, Φ is the incoming muon (anti)neutrino flux and σ is the interaction cross section for electron or muon (anti)neutrinos. The observed event rate at the ND is analogous but does not contain the oscillation probability term. Therefore, measurements at the ND are used to constrain σ and Φ .

Neutrino oscillation probabilities evolve as a function of the ratio of the “baseline” (i.e. the distance the neutrinos travel, a proxy for propagation time) and the neutrino energy (E_ν). Whilst the baselines for LBL experiments are fixed, their neutrino fluxes are typically spread over one-to-several GeV and so the oscillation probability inferred in Equation 1 is the probability *averaged* over the neutrino flux shape. However, a precise characterisation of neutrino oscillations requires inference of the neutrino oscillation probability as a function of E_ν .

A measurement of $N_{FD}(E_\nu)$ would directly characterise $P^{osc}(E_\nu)$ to the extent that $\sigma(E_\nu)$ and $\Phi(E_\nu)$ can be constrained. Unfortunately, in current and planned LBL experiments, the neutrino energy cannot be perfectly reconstructed or known a priori. Instead, experiments attempt to infer this by performing measurements of the final-state products of each neutrino interaction within the FD (here denoted as \vec{x}), which significantly complicates oscillation measurements. Still neglecting backgrounds and detector effects, a differential event rate with respect to \vec{x} can be written as¹:

$$\frac{dN^{FD}}{d\vec{x}} \propto \int dE_\nu \Phi(E_\nu) \sigma(E_\nu, \vec{x}) M(\vec{x} | E_\nu) P^{osc}(E_\nu), \quad (2)$$

where $M(\vec{x} | E_\nu)$ is a matrix mapping between \vec{x} , the measured final state properties and the neutrino energy. It should be noted that the cross section itself also depends on \vec{x} , further complicating the relationship between the differential event rate and the oscillation probability.

From Equation 2 it is clear that, even in this idealised case, a precise inference of the oscillation probability as a function of neutrino energy requires tight control of the incoming neutrino flux normalisations and shapes; the cross section as a function of the measured outgoing particle kinematics; and the mapping between the measured kinematics to the true neutrino energy. To avoid prematurely limiting the reach of DUNE and Hyper-K, which are expecting to collect $\mathcal{O}(10^4 - 10^5)$ events in their FD event samples [2, 4], each of these must be constrained at the few-percent level.

In this work, we specifically characterise the physics that determines M for the DUNE and Hyper-K primary neutrino energy estimation methods, building on previous work that has focussed on the impact of specific physics effects on one of the two [11, 12, 13, 14, 15, 16, 17]. We show that achieving the ultimate precision neutrino oscillation measurements targeted by the two experiments requires the neutrino energy estimation scale to be known at the few-MeV level. Afterwards, we show that *final-state interactions* (FSI), which describe the reinteractions of hadrons produced in neutrino-nucleus scatters with the residual nucleus, introduce changes which impact the neutrino energy scale precision. We then quantify which aspects of FSI modelling which drive uncertainties in neutrino energy estimation for Hyper-K and DUNE, before contrasting the predictions of widely used semi-classical simulations with fully quantum-mechanical microscopic models. Finally, we discuss the implications of our results with the aim of informing how future dedicated measurements can constrain M at the level required for next-generation LBL experiments.

2 Analysis tools and methods

In the few-GeV regime where DUNE and Hyper-K seek to measure neutrino oscillations, neutrinos primarily interact with nuclei. In this work, we simulate these interactions using state-of-the-art neutrino interaction Monte-Carlo event generators. We use the NuWro 25.03.1 [18, 19, 20], GENIE v3.02.00 [21, 22] and NEUT 6.1.3 [23, 24, 25] event generators. These simulate each of the several contributing interaction channels at few-GeV neutrino energies [26, 27]. Figure 1 shows a comparison of the total cross section for different charged-current (CC) processes, as predicted by the NuWro. The four dominant interaction channels at DUNE and Hyper-K energies are: CC quasi-elastic (CCQE) interactions, in which a neutrino interacts with a bound nucleon within a nucleus and produces a charged lepton of the same flavour as the neutrino and a nucleon in the final state; multi-nucleon interactions, in which neutrinos interact with a correlated set of nucleons (CCnph, n-particle-n-hole interactions which are dominated by the CC2p2h contribution); CC resonant pion production (CCRPP), in which the struck nucleon is excited to a higher resonance

¹Subscripts indicating the neutrino flavour and sign are dropped for legibility but would remain as in Equation 1.

(most often a $\Delta(1232)$ baryon) which decays to usually produce a pion and a nucleon; and more inelastic interactions that begin to resolve nucleon quark structure which we refer to with the umbrella term CCDIS (for deep inelastic scattering, although exact definitions for this category vary [28]). For Hyper-K (Figure 1a and Figure 1b), the dominant interaction channel is CCQE, but there are non-negligible contributions from CCnph and CCRPP. For DUNE (Figure 1c and Figure 1d), CCQE, CCRPP and CCDIS all contribute significantly and similarly to the total cross section [2].

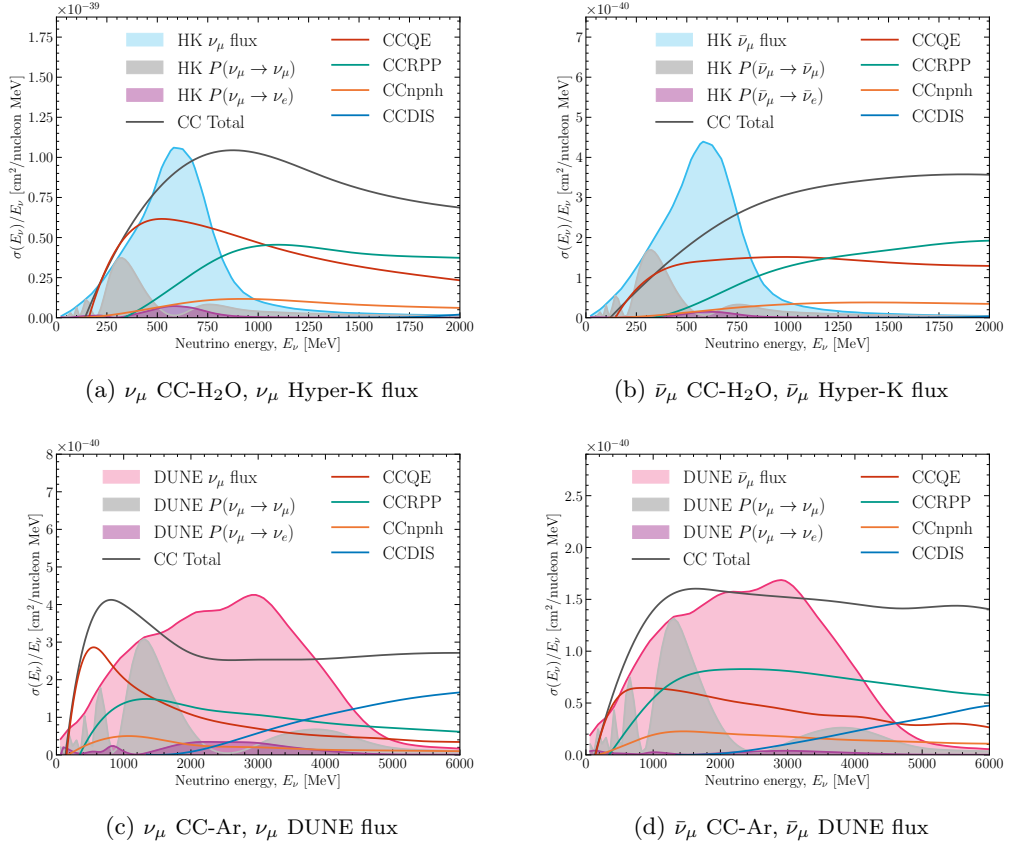


Figure 1: The neutrino and antineutrino CC inclusive cross section on water and argon targets predicted by the NuWro simulation overlaid with the corresponding predicted neutrino fluxes from the Hyper-K and DUNE FD before and after considering neutrino oscillations (using the parameters given in Table 1). The contribution to the cross section is broken down by neutrino interaction channel. Small contributions from coherent pion scattering are not shown.

2.1 Modelling final state interactions with Monte Carlo generators

Most event generators employ a factorised description of a neutrino interaction, where a neutrino interaction “hard scatter” is first simulated to produce hadrons within the target nucleus which are subsequently transported out, possibly re-interacting as they propagate, via a separate FSI routine. This approach uses semi-classical intranuclear cascade (INC) models to describe the FSI, which transport hadrons through the nucleus in discrete steps [29, 30, 31]. An alternative approach, only recently implemented in generators, is a microscopic quantum mechanical calculation of cross section that considers FSI by calculating the outgoing hadronic wavefunctions in a nuclear potential [32, 33]. In this section, we will first detail these two different approaches to simulating FSI in neutrino generators, and then describe the generator configurations chosen for the rest of this work.

2.1.1 Semi-classical intranuclear cascades

INCs simulate FSI by transporting the outgoing hadrons through the residual nucleus using semi-classical methods. Each hadron is propagated as a classical particle whose interaction probability at every step is set by a local mean free path, computed from in-medium effective cross sections. At each interaction point, the hadron may scatter elastically, undergo charge exchange, be absorbed, or produce additional particles, with the

choice of fate sampled probabilistically. Each additionally created particle is also propagated through the INC. By construction, the INC only redistributes energy and particle content among the final-state hadrons, leaving the cross section as a function of outgoing lepton kinematics for any interaction channel unchanged.

Most INC implementations used in neutrino event generators are “space-like” cascades, in which each hadron is propagated through the nucleus in discrete spatial steps, with the local interaction probability re-evaluated at each step. This is the approach used by both NEUT [25] and NuWro [18], as well as the hA2018 and hN2018 models in GENIE [22]. An alternative class of “time-like” cascades evolves the projectile and all spectator nucleons simultaneously in steps of space and time. The INCL++ model [34, 35], available in GENIE, is an example of a time-like cascade and is additionally able to describe processes that are often neglected in space-like frameworks, such as nuclear cluster emission. Once the cascade is complete, INCs can be coupled to a nuclear de-excitation routine (e.g. ABLA [36]) which dissipates the residual excitation energy of the remnant nucleus via the emission of additional particles, including nucleons or nuclear fragments. A comparison of many of these INC models can be found in Ref. [29] and an additional review is provided in Ref. [11].

A well-known shortcoming of INC treatments is that they are applied incoherently on top of a hard-scatter cross section that is itself derived under generally different assumptions about the nuclear medium [29]. This inconsistency between the initial interaction and the subsequent transport is a known source of theoretical uncertainty in any INC-based prediction. We note that there are some generators in which the treatment of FSI and the underlying nuclear model is fully consistent, such as GiBUU [37] and Achilles [38].

2.1.2 Microscopic calculations Microscopic calculations of FSI aim to fix the issue of inconsistency that is present in INCs. In this case, the model calculates the hadron current from the bound- and scattered-state wavefunctions. The scattered-state wavefunctions are solutions to a wave equation including the nuclear potential, thus encoding the effect of the residual nuclear medium on the hadron dispersion relation. This is done in a consistent quantum mechanical and relativistic framework. This approach, when used with a real nuclear potential, encodes the case where the scattered hadron interacts with the residual nuclear medium and changes momentum and direction, but does not produce additional particles (coined “elastic FSI”) [39]. When a complex nuclear potential is used, it also encodes the flux lost to inelastic processes and, in the CCQE case, constitutes an absolute lower bound of the cross section. However, this approach is not without drawbacks. Due to the complexity of calculating the scattered-state wavefunctions, it is computationally expensive. Additionally, effects such as additional nucleon creation, ejection and pion absorption are not simulated. Despite this, this approach has been implemented in the NEUT event generator via precomputed hadron tensor tables [32]. The approach is coupled with the NEUT INC to simulate both the elastic FSI from the microscopic calculation and the inelastic FSI from the NEUT INC. The NEUT INC has no inherent elastic FSI and, if one uses a real nuclear potential in the microscopic calculations, there is no danger of double-counting FSI effects.

2.2 Event generator details

As discussed, we consider simulations of neutrino interactions expected within DUNE and Hyper-K using the NuWro, GENIE and NEUT event generators. We use NuWro as our baseline simulation, GENIE to examine variations in simulations from a wide variety of INC models, and NEUT to consider microscopic FSI treatments.

We simulate ν_μ and $\bar{\nu}_\mu$ interactions to be representative of those seen at DUNE and Hyper-K separately. For the DUNE case, we consider interactions using the experiment’s ν_μ and $\bar{\nu}_\mu$ fluxes [40] in neutrino-enhanced and antineutrino enhanced beam modes respectively. For DUNE we consider all simulated CC interactions, as this is the signal topology for the experiment’s oscillation analysis [2]. For the Hyper-K case, we generate analogous (anti)neutrino-water interactions using the T2K experiment’s public flux [41] (which uses the same neutrino beam as Hyper-K). For Hyper-K, we consider only CC interactions with no pions in the final state (CC0 π interactions) as the experiment’s primary neutrino oscillation signal topology [4]. Neutrino oscillations are applied via a reweighting of the input simulations using the `OscProb` framework [42], using the nominal parameters shown in Table 1, taken from Ref. [9, 43]² but with δ_{CP} set to $-\pi/2$. All generator output is processed using NUISANCE [45] into a common event format. In this work, we do not simulate contributions to DUNE and Hyper-K event rates due to

²This parameter set corresponds to the NuFit 6.0 normal-ordering best fit without SK-atmospheric and IceCube-24 data [44].

backgrounds from topologies outside of the primary signal (e.g. the $CC1\pi$ background for Hyper-K or neutral current backgrounds) or from beam contamination (e.g. the ν_μ contributions to antineutrino enhanced running mode). We also do not consider detector smearing or inefficiency.

Parameter	Value
θ_{12} [rad]	0.58784
θ_{13} [rad]	0.14870
θ_{23} [rad]	0.84649
Δm_{21}^2 [eV ²]	7.49×10^{-5}
Δm_{32}^2 [eV ²]	2.459×10^{-3}
δ_{CP}	$-\pi/2$
Mass Ordering	Normal Ordering

Table 1: Oscillation parameters used in the simulations, taken from Table 14.7 in the PDG 2025 review of neutrino masses, mixing and oscillations (Ref. [9, 43]), corresponding to the NuFit 6.0 normal-ordering best fit without SK-atmospheric and IceCube-24 data [44]; δ_{CP} is fixed to $-\pi/2$ for the purposes of this work.

2.2.1 NuWro CCQE interactions are simulated using a spectral function approach based on Refs. [46, 12] for water and on Refs. [47, 48, 49] for argon. Two- and three-body current (CC2p2h and CC3p3h respectively) interactions are simulated with the model from the Valencia group [50, 51]. Pion production below the deep inelastic scattering (DIS) region is simulated with the Hybrid model from the Ghent group [52]. DIS generation uses the GRV98 parton distribution functions with Bodek-Yang corrections [53, 54] together with PYTHIA [55] for hadronisation at high hadronic invariant mass ($W > 1.9$ GeV/ c^2). For intermediate hadronic masses, $1.6 < W < 1.9$ GeV/ c^2 , NuWro implements a linear transition between the Hybrid and DIS models. FSI are simulated using NuWro’s custom INC [18], a space-like cascade that uses the Salcedo-Oset model [30] for low-energy pion-nucleus interactions and free NN cross sections, with in-medium corrections, for nucleon reinteractions.

2.2.2 GENIE In addition to NuWro, we also use simulations from the GENIE generator, provided in Refs. [56, 57], to study the effect of more substantial changes to the INC model. GENIE is a widely-used neutrino generator (notably in LAr-based experiments) and has a broad range of available models and tunes. GENIE is the only neutrino generator to provide four different INC models which can be combined with different hard scatter models.

To describe primary interactions, we use the G18_10a_00_000 GENIE configuration [58], which uses a local Fermi gas nuclear ground state and the model from the Valencia group for CCQE and CCnph interactions [59, 60, 61], although for CCnph it uses an older version of the model than is in NuWro and only considers the CC2p2h channel. For CCRPP interactions, GENIE uses the Berger-Sehgal pion production models [62, 63], and for DIS it uses the GRV98 parton distribution functions with Bodek-Yang corrections [53, 54]. Hadronisation is modelled either with PYTHIA [64, 55] (at invariant masses, $W > 3.0$ GeV/ c^2), the custom AGKY model [65] ($W < 2.3$ GeV/ c^2), or an interpolation between them [66]. Four samples are generated with this hard-scatter configuration held fixed, each using a different INC available within GENIE: the default hA2018 model [58], the hN2018 model [58], the Liège Intranuclear Cascade model (INCL) [35], and the GEANT4 Bertini Cascade model (G4BC) [67], the latter accessed through GENIE’s dedicated interface [68]. These cascades differ substantially in the physics choices they make. Very broadly, hA2018 and hN2018 are widely-used models that are tuned extensively to hadron scattering data, while INCL and G4BC are more sophisticated hadron transport models with a more careful treatment of the nuclear medium and a richer set of final-state channels. Further details and comparisons of these FSI models are available in Refs. [29, 69, 11]. Holding the hard-scatter model fixed across the four samples ensures that any variation between them is attributable to the INC alone. We note that the hA2018 and hN2018 models share much of their pion FSI treatment with the NEUT and NuWro cascades.

2.2.3 ED-RMF in NEUT We use the NEUT event generator in order to access its implementation of microscopic FSI model calculations for CCQE interactions, recently implemented and detailed in Ref. [32]. In this model, bound- and final-state wavefunctions are used to define the hadron current, which is then used to describe the hadron tensor as a sum of single

particle relativistic mean field (RMF) states. The final-state wavefunctions are solutions to the Dirac equation in the presence of a relativistic nuclear potential. Doing this encodes elastic FSI into the final-state particle information which is then used to seed the NEUT INC and perform inelastic FSI. It has been shown that using real relativistic nuclear potentials poses little risk of double counting FSI effects with such INCs [39]³. The nuclear potentials shown in this work are the energy-dependent RMF (ED-RMF) [70, 71] and relativistic plane-wave impulse approximation (RPWIA). The RPWIA model considers no nuclear potential for the scattered nucleon, and so is a useful reference model without a microscopic FSI treatment. The ED-RMF potential is constructed by applying a softening function to the energy-independent RMF potential of the bound-state system [72]. The softening function is a function of scattered nucleon kinetic energy (T_N) and at low values of T_N it is close to one; this ensures that the initial and final states are solutions to the same Dirac equation and encodes natural Pauli blocking. This model, due to its computational complexity, is currently only implemented for CCQE interactions.

3 Neutrino energy estimation

LBL experiments usually use one of two classes of methods for neutrino energy estimation. This choice is tailored to their detector technology and the ranges of neutrino energies they cover.

3.1 Kinematic neutrino energy estimation

The kinematic method of neutrino energy estimation infers neutrino energy from the kinematics of outgoing particles under some set of approximations. Its most common application derives an estimator for neutrino energy, E_ν^{QE} , by assuming that an incoming neutrino undergoes a CCQE interaction with a single neutron at rest within the nucleus which is subject to some fixed nuclear binding energy, E_b :

$$E_\nu^{\text{QE}} = \frac{m_p^2 - m_\ell^2 - (m_n - E_b)^2 + 2E_\ell(m_n - E_b)}{2(m_n - E_b - E_\ell + p_\ell^z)}. \quad (3)$$

Here $m_{p/\ell/n}$ is the mass of a proton, outgoing lepton or neutron; and E_ℓ and p_ℓ^z are the outgoing lepton energy and projected lepton momentum along the direction of the incoming neutrino, respectively. E_b is the mean nuclear binding energy and is set to 27 MeV in this work. For antineutrino interactions the proton and neutron masses are swapped. This form of kinematic energy estimation only requires the reconstruction of the outgoing lepton kinematics, making it applicable in water Cherenkov detectors where outgoing hadrons may be below the Cherenkov threshold. Since it is built assuming a CCQE interaction, it is usually only applied to subsamples of identified interactions that contain a high proportion of CCQE events and so is best suited for experiments with neutrino beams with energies predominantly below the point at which other channels become dominant ($\lesssim 1$ GeV). In the context of T2K and Hyper-K, which share a neutrino beam peaked at ~ 0.6 GeV, Equation 3 is applied to a selection of CC0 π interactions⁴ which are predicted by the NuWro simulation to contain 78.7% (85.1%) of ν_μ ($\bar{\nu}_\mu$) CCQE interactions and make up 61.0% (72.1%) of the total CC event rate considering the (anti)neutrino enhanced flux.

3.2 Calorimetric neutrino energy estimation

Experiments with an FD capable of low-threshold particle tracking and calorimetry can use alternative metrics to estimate neutrino energy, based on summing energy deposits within their detectors. This applies to the Liquid Argon TPC of the DUNE experiment as well as the scintillator detectors of the NOvA experiment, which are both sensitive to the energy that charged particles leave inside the detector down to negligible threshold. Neglecting very rare events with heavy mesons and baryons, a common variable used to estimate the energy recorded by calorimetrically summing energy deposits is:

$$E_\nu^{\text{avail}} = E_\ell + \sum_{i=p,\pi^\pm} T_i + \sum_{i=\pi^0,\gamma,e^\pm} E_i. \quad (4)$$

Here, E_ν^{avail} is the estimated neutrino energy approximated as the outgoing lepton energy plus the sum of the kinetic energies of protons and charged pions and the sum of the total energy of neutral pions and photons. This variable was first introduced in Ref. [74]. Only the kinetic energy

³It is important to note that this is only true if the event generator does not have a dedicated elastic rescattering calculation in the INC, or it is turned off, as is the case for NEUT.

⁴Whilst not considered in this work, within T2K a modified version of the Equation 3 formula is applied to a subsample of interactions rich in pion production by replacing the proton mass by the $\Delta(1232)$ mass [73].

of protons is considered as their mass energy is already present in the initial state of the interaction⁵. The same applies to light nuclear fragments produced in the interaction (deuterons, tritons and α particles), which contribute only their kinetic energy. Neutrons are assumed to not deposit any energy within the detector that can be associated with the interaction. The total energy of neutral pions is included because their kinetic and mass energy is converted to photons in a prompt decay and the latter subsequently deposit almost their total energy in the detector following electron-positron pair production. Charged pions undergo frequent secondary interactions and partially decay to neutrinos. Equation 4 makes a conservative assumption that none of the pions' mass energy is visible. Very small contributions from heavier nuclear remnants, hyperons and any other heavy mesons and baryons are neglected in the formula for this work.

At the other extreme, an alternative neutrino energy estimator could be written as:

$$E_{\nu}^{\text{had}} = E_{\ell} + \sum_{i=p} T_i + \sum_{i=\pi^{\pm}, \pi^0, \gamma, e^{\pm}} E_i, \quad (5)$$

where the total charged pion energy is considered. As in E_{ν}^{avail} , protons and light nuclear fragments enter only through their kinetic energy and heavier hadrons are neglected. It is likely that the true visible energy deposit within a DUNE TPC lies somewhere between the two. The two estimators are contrasted and further discussed in Ref. [75].

3.3 Neutrino energy estimation and precision oscillation measurements

Precise neutrino energy estimation is needed to accurately infer neutrino oscillation parameters from the shape of the oscillated neutrino spectra seen in LBL experiments. Within the three-flavour PMNS neutrino mixing framework, this is especially relevant for measurements of Δm_{32}^2 and δ_{CP} , particularly when the latter is close to values of $\pm\pi/2$ (implying maximal CP violation). Modifications to these parameters have a significant impact on the oscillated spectra shape [4, 2]. To demonstrate this, Figure 2a, Figure 2c and Figure 3a, Figure 3c show the projected event rate of muon ($N_{FD}^{\nu_{\mu}}$) or electron neutrino ($N_{FD}^{\nu_e}$) CC0 π interactions as a function of *true* neutrino energy using the Hyper-K and DUNE fluxes respectively. The integrated event rates have been scaled to approximately 10 years of expected data taking according to the numbers provided in Refs. [2, 4], which amounts to a total ν_{μ} event rate of 13436 and 8845, and an oscillated ν_e rate of 2591 and 2475 for DUNE and Hyper-K respectively. NC backgrounds, wrong-sign contaminations and intrinsic ν_e contributions are ignored. In these figures, the baseline NuWro simulation has been reweighted to consider small variations of either Δm_{32}^2 ($\pm 0.4\%$) or δ_{CP} ($\pm 20^\circ$) around the nominal neutrino oscillation probability considered, which closely corresponds to the experiments' target precisions [4, 2]. This illustrates that the position of the oscillation maximum in the FD muon neutrino spectra is sensitive to variations of Δm_{32}^2 , whilst the peak position of the electron neutrino appearance spectra is sensitive to changes in δ_{CP} . This stems directly from the neutrino oscillation probability. The leading-order disappearance probability:

$$P(\nu_{\mu} \rightarrow \nu_{\mu}) \simeq 1 - \sin^2 2\theta_{23} \sin^2 \left(\frac{\Delta m_{32}^2 L}{4E_{\nu}} \right), \quad (6)$$

depends on Δm_{32}^2 only through the combination Δm_{32}^2 and L/E_{ν} , so changing Δm_{32}^2 shifts the position of oscillation dip along the energy axis. The shift is larger at low E_{ν} and reverses sign on either side of the dip, so Δm_{32}^2 is read off from the position of the suppression and cannot be absorbed by an overall change in normalisation. In the appearance channel, the leading order δ_{CP} -dependent interference term of the oscillation probability can be written compactly as:

$$\Delta P_{\delta_{\text{CP}}}(\nu_{\mu} \rightarrow \nu_e) \propto \cos \left(\frac{\Delta m_{32}^2 L}{4E_{\nu}} + \delta_{\text{CP}} \right), \quad (7)$$

so δ_{CP} enters as a phase shift of an argument which depends on $1/E_{\nu}$. The observable response to δ_{CP} is the change in oscillation probability which manifests as a change in the observed event rate. This change corresponds to the derivative of Equation 7:

$$\frac{\partial \Delta P_{\delta_{\text{CP}}}}{\partial \delta_{\text{CP}}} \propto -\sin \left(\frac{\Delta m_{32}^2 L}{4E_{\nu}} + \delta_{\text{CP}} \right), \quad (8)$$

and whether a small change in δ_{CP} resembles a rate change or a shape change is decided by the symmetry of this function about the first oscillation maximum, where $\Delta m_{32}^2 L/4E_{\nu} = \pi/2$. At

⁵The effects of the 1.3 MeV proton-neutron mass difference and nuclear binding energy are neglected here

$\delta_{\text{CP}} = 0$ or π the derivative is $\mp \sin(\Delta m_{32}^2 L/4E_\nu)$, which is symmetric about the maximum and largest there: a shift in δ_{CP} moves the event rate at the oscillation peak and changes both sidebands in the same direction, mimicking a normalisation change. At $\delta_{\text{CP}} = \pm\pi/2$ (i.e. maximal) the derivative is $\mp \cos(\Delta m_{32}^2 L/4E_\nu)$, which is antisymmetric about the energy of the oscillation peak and vanishes there. A shift in δ_{CP} leaves the peak rate unchanged and instead moves the probability along the neutrino energy axis. This distortion is therefore largest precisely when CP violation is maximal, but it is identical for $+\pi/2$ and $-\pi/2$, so determining the sign of δ_{CP} requires input from the antineutrino spectrum, in which the $\sin \delta_{\text{CP}}$ term enters with the opposite sign. Implications of oscillation-parameter and energy-scale variations on the antineutrino oscillation spectra and on the ratios of ν_e to $\bar{\nu}_e$ appearance events are discussed in [Appendix A](#).

[Figure 2b](#), [Figure 2d](#) and [Figure 3b](#), [Figure 3d](#) show the event rate as a function of a neutrino energy estimator (E_ν^{QE} and E_ν^{had} for the Hyper-K and DUNE cases, respectively) rather than true neutrino energy. This demonstrates that Δm_{32}^2 and δ_{CP} affect the shape of the FD muon and electron *estimated* neutrino energy spectra similarly to the *true* one. The figures also show alternative estimated energy spectra in which the nominal oscillation parameters are used but the neutrino energy estimators are biased by a constant 5 MeV for the Hyper-K case or 15 MeV for the DUNE case. These numbers were chosen empirically, but they broadly correspond to a shift of 0.5% of the means of DUNE and Hyper-K energies. It is clear that the difference between the nominal and alternative reconstructed energy spectra is comparable to the difference between the nominal and altered values of Δm_{32}^2 and δ_{CP} , giving an approximate scale for the precision with which the neutrino energy scale must be controlled. Overall, this illustrates the importance of constraining neutrino energy estimation at the 5-15 MeV level for next-generation LBL experiments to meet their ultimate precision goals⁶.

⁶Whilst the focus of this work concerns how FSI modelling might introduce neutrino energy scale uncertainties, it is the overall energy scale uncertainty that must be kept to the 5-15 MeV level. This can have contributions from other nuclear effects or from the detector smearing.

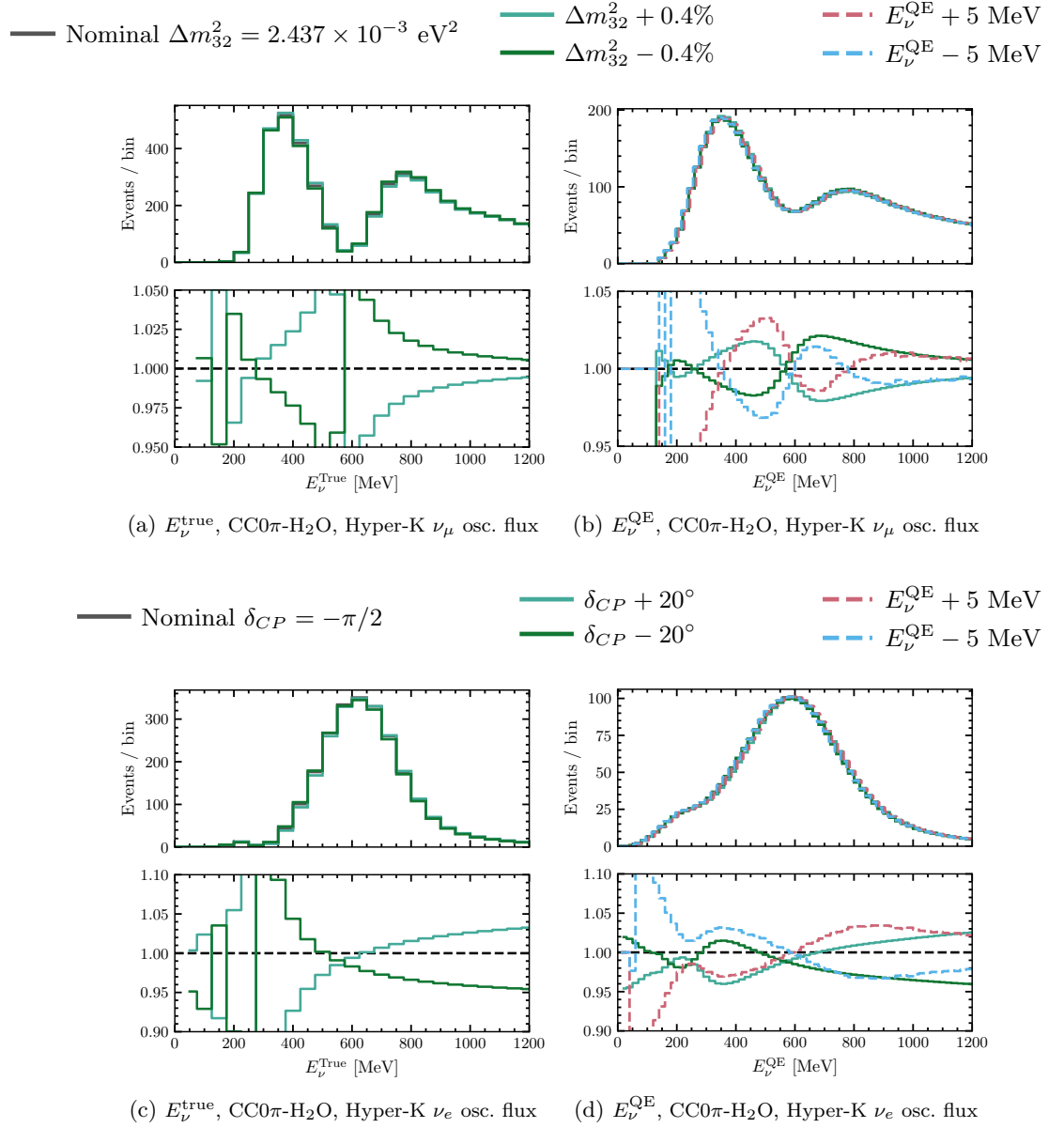


Figure 2: The NuWro simulated rate of CC0 π ν_μ or ν_e interactions on water at the Hyper-K FD using the oscillated Hyper-K flux (see Table 1) as a function of true (E_ν^{true}) or estimated (E_ν^{QE}) neutrino energy. For the former, variations of oscillation parameters corresponding to the Hyper-K ultimate target precision are shown. For the latter, these are compared to E_ν^{QE} biased by ± 5 MeV.

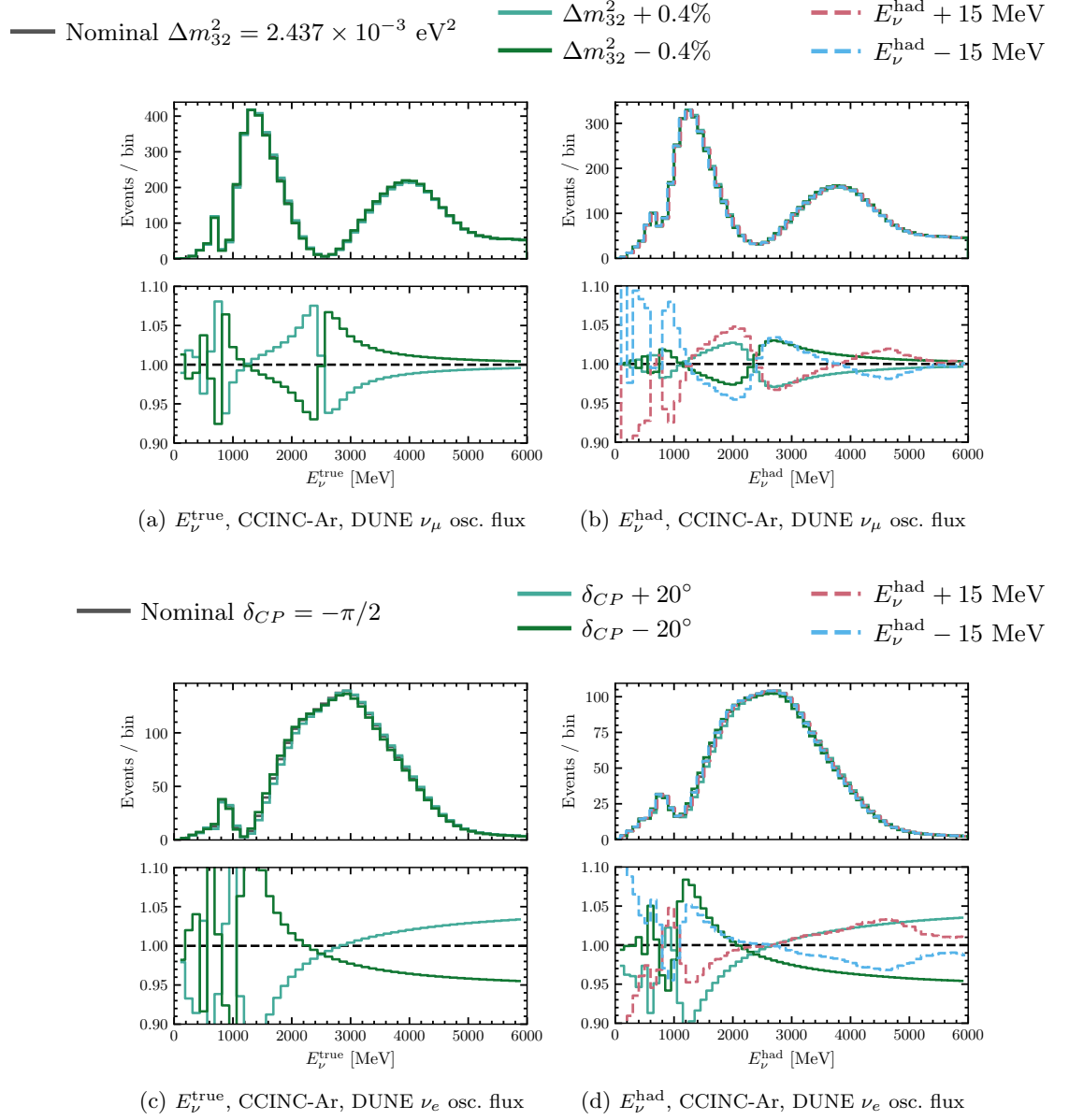


Figure 3: The NuWro simulated rate of CC inclusive ν_μ or ν_e interactions on argon at the DUNE FD using the oscillated DUNE flux (see Table 1) as a function of true (E_ν^{true}) or estimated (E_ν^{had}) neutrino energy. For the former, variations of oscillation parameters corresponding to the DUNE ultimate target precision are shown. For the latter, these are compared to E_ν^{had} biased by $\pm 15 \text{ MeV}$.

4 The impact of FSI on neutrino energy estimation

In this section, we describe how FSI affects the neutrino energy estimators introduced in [section 3](#). We first characterise their performance in the absence of FSI, then show how FSI modifies it, and finally isolate specific FSI processes to quantify their impact. The performance of the estimators is set by the hadronic system and the estimator definition, and is essentially independent of the outgoing lepton flavour; we therefore use muon (anti)neutrinos throughout, averaging over the oscillated ν_μ ($\bar{\nu}_\mu$) flux for the neutrino(antineutrino) case, with the $\nu_e/\bar{\nu}_e$ results being very similar. We discuss the implications of the muon-versus-electron oscillated spectra choices in [section 5](#).

4.1 Neutrino energy estimation bias without FSI

[Figure 4](#) and [Figure 5](#) show the difference between true neutrino energy and the neutrino energy estimators introduced in [section 3](#) (E_ν^{QE} for Hyper-K, E_ν^{avail} and E_ν^{had} for DUNE), henceforth referred to as the energy estimation *bias*, using NuWro simulations without any FSI for the Hyper-K and DUNE case respectively. These and subsequent distributions are shown as differential cross sections with respect to the energy estimation bias, which is proportional to the probability of finding an interaction with a particular bias. The distributions are shown separately for neutrino and antineutrino interactions, broken down by contributions that help characterise the physics responsible for the imperfect energy estimation even before FSI.

The bias in the neutrino energy estimation directly stems from the approximations made in building the estimators. In the case of E_ν^{QE} , [Equation 3](#) is built assuming a CCQE interaction on a stationary nucleon with some fixed binding energy. Most of the time, none of these conditions are entirely met, causing the bias shown in [Figure 4](#). Firstly, nucleons in the nucleus are not stationary, they move with some *Fermi motion* which is isotropic and distributed between 0 and ~ 230 MeV/c [76]. This motion causes interactions to have their energy misestimated by the momentum of the struck nucleon before the interaction takes place and is responsible for the majority of the spread seen for CCQE interactions. Secondly, nucleons inside the nucleus do not have a single fixed nuclear binding energy but rather have a distribution of possible values (see e.g. Ref.[46]). This causes a further small spread (at a maximum of the few 10s of MeV scale of binding energies) and a potential non-zero mean bias if the average real binding energy is not the E_b assumed in [Equation 3](#). Thirdly, it is not possible to isolate a pure sample of CCQE events. Even for CC0 π interactions with no FSI, interactions with bound states of multiple nucleons (CCn π nh interactions) leave final states that can be indistinguishable from CCQE interactions. Since [Equation 3](#) assumes an interaction with a single target nucleon, the energy of CCn π nh interactions is estimated incorrectly. The bias seen is similar for neutrino and antineutrino interactions, with the main differences driven by the slightly changing fraction of CCQE to CCn π nh interactions. The small bump in [Figure 4b](#) at ~ -200 MeV is due to Λ^0 producing interactions.

There is one case where the E_ν^{QE} formula is almost exact: when an antineutrino interaction happens on a hydrogen atom (which is the case for slightly less than 2/18 of the interactions on a water target), which is not subject to nuclear effects. In this case E_ν^{QE} estimates the neutrino energy perfectly except for an offset related to the chosen value of the binding energy in [Equation 3](#) (as hydrogen should have zero binding energy). This contribution is clearly visible in [Figure 4b](#) as a large peak centred at a value corresponding to the difference between [Equation 3](#) evaluated with $E_b = 0$ MeV and the chosen value of 27 MeV.

In contrast, E_ν^{avail} and E_ν^{had} assume that all charged particle energy deposited in a detector is identified and so the bias observed in [Figure 5](#) is from unaccounted energy from other sources. The dominant contribution is from energy that goes unseen as it is lost to final-state neutrons. This is typically a much larger fraction of the total interaction energy for antineutrino interactions than for neutrino interactions (this is clearly shown by comparing [Figure 5a](#) and [Figure 5c](#) to [Figure 5b](#) and [Figure 5d](#)). Beyond neutrons, energy lost to overcoming nuclear binding energy is also unseen, causing biases at the level of 10-50 MeV, which dominates the no neutron contribution to [Figures 5c](#) and [5d](#). For [Figures 5a](#) and [5b](#) the mass energy of charged pions is also assumed to go unseen. This causes additional bias in discrete units of pion masses, seen very clearly for neutrino interactions. This additional bias also affects antineutrino interactions, but discrete peaks in the bias are not so obvious as their impact is small relative to the continuous bias driven by energy lost to neutrons. The very small contributions to the no neutron population at large negative bias in [Figures 5c](#) and [5d](#) come from interactions that produce hyperons, causing a bias of at least their mass, as well as other heavy mesons and baryons that are not explicitly accounted for in [Equation 4](#) and [Equation 5](#).

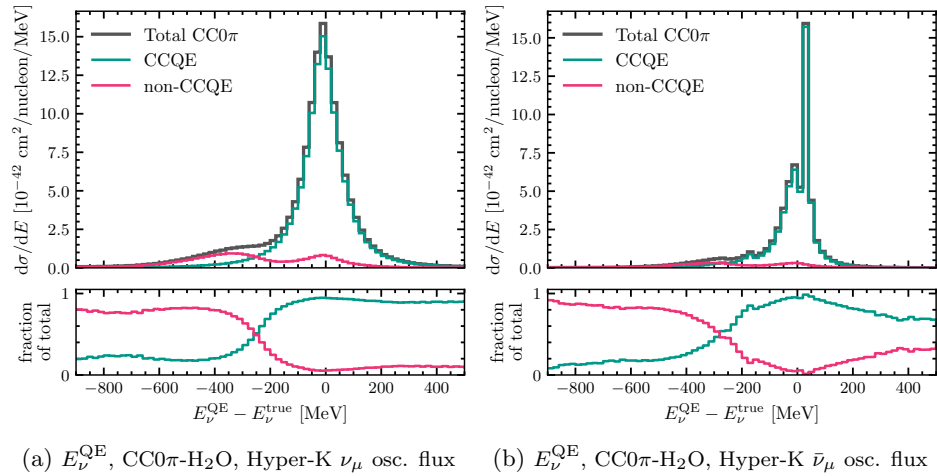


Figure 4: The NuWro simulated neutrino energy estimation bias (using E_ν^{QE}) for CC0 π ν_μ or $\bar{\nu}_\mu$ interactions on a water target at the Hyper-K FD using the oscillated Hyper-K flux (see Table 1), split by contributions from CCQE and non-CCQE interactions.

4.2 The impact of INC FSI

The neutrino energy biases shown in Figure 4 and Figure 5 are significantly modified by consideration of FSI as modelled with INCs. This is demonstrated for the Hyper-K and DUNE cases in Figure 6 and Figure 7 respectively, where the neutrino energy estimation bias is shown for the NuWro model prediction before and after applying an INC.

In the Hyper-K case, since the neutrino energy estimator is built only from lepton kinematics, that are not affected by the INC by construction, the CCQE and CCn π contributions to the neutrino energy bias remain very similar. The most dramatic effect of FSI is instead to add significant extra strength to the distribution where the neutrino energy estimator is ~ 250 - 500 MeV smaller than the true neutrino energy. This contribution has similar strength to the total CCn π component and stems from pion production interactions in which the outgoing pion is absorbed within the residual nucleus as part of the INC, leaving the final state indistinguishable from CCQE interactions. As with CCn π interactions, the bias in the estimator comes from applying Equation 3 to interactions for which it is not applicable⁷. There is also a small additional effect from CCQE or CCn π interactions where outgoing nucleons stimulate pion production through the cascade, moving interactions out of the signal topology for Hyper-K, but this only affects $\sim 1\%$ of these interactions. The impact of the INC is similar for neutrino and antineutrino interactions on complex nuclei (i.e. with $A > 1$). However, the antineutrino interactions on hydrogen are not affected by FSI (since free protons are not bound) so the hydrogen peak in Figure 6b remains unchanged from the one in Figure 4b. Also, for antineutrinos the slightly smaller portion of CCn π events makes the FSI-driven pion absorption contribution to the bias slightly more pronounced.

In the DUNE case, re-scattering of hadrons within the INC alters the outgoing charged pion multiplicity, affecting the bias when using E_ν^{avail} , and the fraction of outgoing energy in neutrons, affecting both E_ν^{avail} and E_ν^{had} . The impact of the former is most clear in Figure 7a, which shows how the application of the INC changes the relative strength of the discrete peaks corresponding to different charged pion multiplicities. The impact of the INC on the fraction of energy carried away by neutrons is more dramatic. The INC often produces additional neutrons in interactions that otherwise had none, causing a strong migration of interactions away from the low-bias (usually zero-neutron) peak to slightly larger biases. This is further demonstrated in Figure 8, which shows the fraction of energy transferred to the hadronic system in a neutrino interaction (q_0) that is given to final-state neutron kinetic energy before and after applying the INC. For neutrino interactions it is clear that FSI simulation via the INC dramatically increases the cross section of interaction topologies containing neutrons, although these neutrons typically take only a small fraction of the energy transfer. This explains the migration of events from the peaks in Figure 7 into adjacent higher-bias regions. For antineutrino interactions the cross section of interaction topologies containing neutrons is more modestly increased and the typical fraction of energy transfer carried

⁷In the case of pion-production at Hyper-K, which usually occurs from interactions that excite struck nucleons into resonant states, the assumption that the interaction is with a neutron is therefore incorrect, and the scale of the bias induced is set by the difference between using m_n and the mass of the excited resonance in Equation 3.

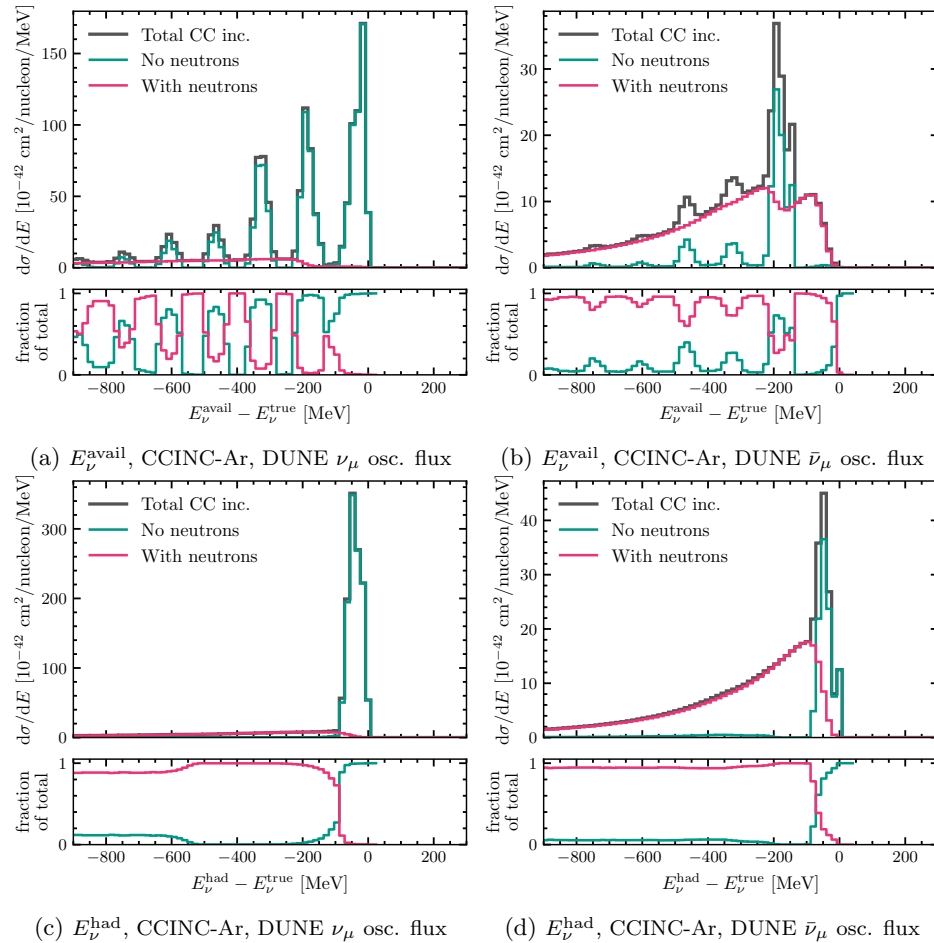


Figure 5: The NuWro simulated neutrino energy estimation bias (using E_{ν}^{had} or E_{ν}^{avail}) for CC inclusive ν_{μ} or $\bar{\nu}_{\mu}$ interactions on an argon target at the DUNE FD using the oscillated DUNE flux (see Table 1), split by contributions from interactions that do and do not produce final state neutrons.

away by neutrons is actually decreased, explaining the smaller change due to the impact of the INC on the energy estimation bias for antineutrino interactions.

Figure 6 and Figure 7 show neutrino energy estimation bias averaged over the oscillated muon (anti)neutrino flux for Hyper-K and DUNE. However, the size and shape of the bias varies with neutrino energy itself and so may differ for variations of neutrino oscillation parameters and between the ND and FD. To illustrate the magnitude of this effect, Figure 9 and Figure 10 show the evolution of the neutrino energy estimation bias as a function of neutrino energy for the Hyper-K and DUNE cases respectively. It is clear that larger biases are more likely when neutrino energies are larger, primarily driven by the changing contribution from different interaction channels (as demonstrated in Figure 1). For Hyper-K this is because the bias stems from CCnpn and pion-producing interactions which both have cross sections that grow faster than the CCQE one above ~ 0.5 GeV neutrino energy, making their relative contribution to CC0 π interactions increase above this. For DUNE a similar argument applies where higher energy transfer interactions, which can produce higher energy neutrons and higher charged pion multiplicities, become more likely at larger neutrino energies. The same qualitative conclusions apply for both neutrinos and antineutrinos.

4.3 FSI beyond the INC

As discussed in section 2, the semi-classical approach of INCs does not consider the full impact of FSI that is captured by modern microscopic models. The latter consider an additional facet of FSI through the incorporation of a nuclear potential that distorts the outgoing nucleon wavefunction in the cross-section calculation, as described in subsection 2.2.3. The impact of this potential can be quantified by comparing the neutrino energy estimator bias for NEUT simulations using the ED-RMF model (which includes this potential) and the RPWIA model (which neglects it but is

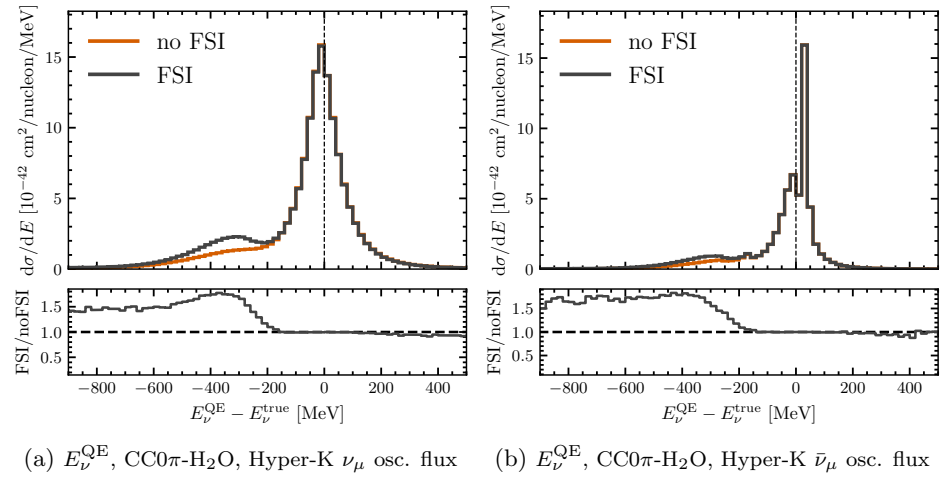


Figure 6: The NuWro simulated neutrino energy estimation bias (using E_ν^{QE}) for CC0 π ν_μ or $\bar{\nu}_\mu$ interactions on a water target at the Hyper-K FD using the oscillated Hyper-K flux (see [Table 1](#)), split for cases when the NuWro INC is and is not applied.

otherwise equivalent). This is shown for neutrino CCQE interactions in [Figure 11](#), for an argon and water target for the cases of DUNE and Hyper-K respectively⁸. The RPWIA model using an argon target includes only neutrino inputs at the time of writing; therefore, only neutrino interactions are generated here.

Since the consideration of the nuclear potential in ED-RMF does not directly stimulate neutron or pion production, the DUNE estimators are not very sensitive to differences between ED-RMF and RPWIA. Conversely, [Equation 3](#) is very sensitive to the alteration of interaction kinematics for CCQE interactions between ED-RMF and RPWIA, causing a significant shift in the bias distribution. This shift originates from the nuclear mean-field potential, which modifies the initial- and final-state nucleon kinematics, indirectly altering the scattered lepton kinematics through energy-momentum conservation. In the RPWIA case, this does not occur and [Equation 3](#) is expected to be symmetric about zero bias. Similar effects have previously been reported in Ref. [\[12\]](#).

⁸For neutrino interactions, no CCQE interactions can occur on hydrogen atoms, so all interactions shown here are in fact on oxygen.

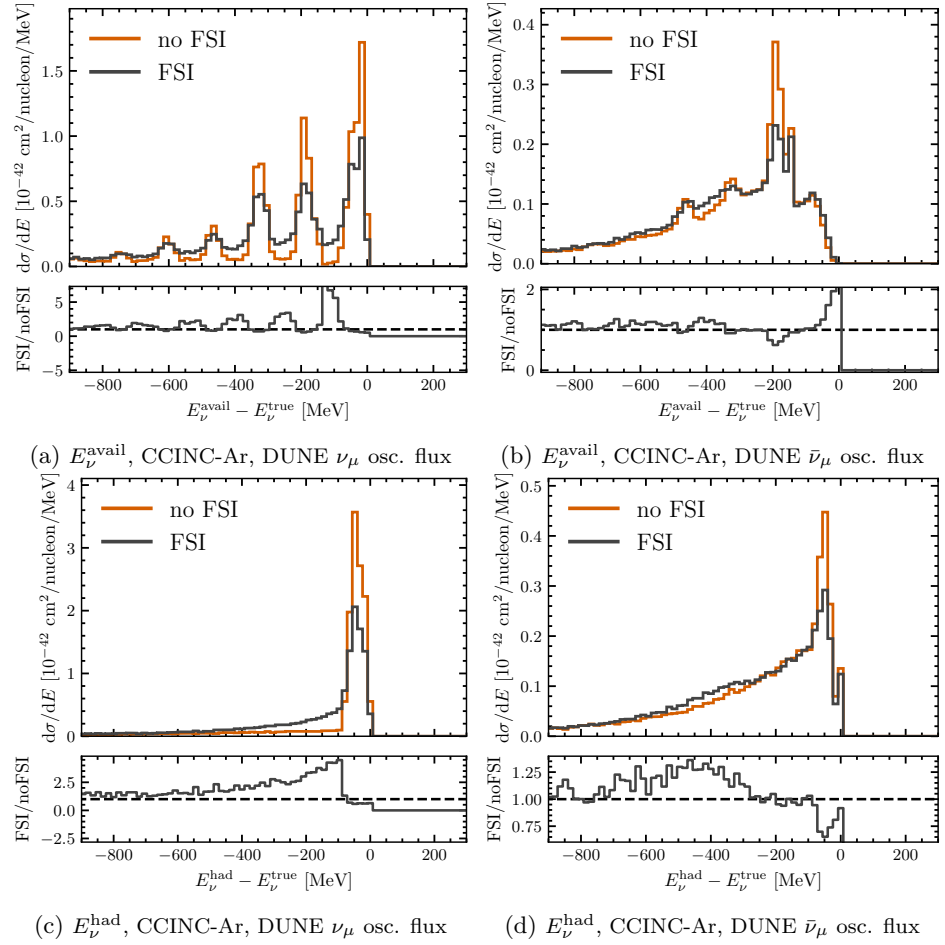


Figure 7: The NuWro simulated neutrino energy estimation bias (using E_{ν}^{had} or E_{ν}^{avail}) for CC inclusive ν_{μ} or $\bar{\nu}_{\mu}$ interactions on an argon target at the DUNE FD using the oscillated DUNE flux (see [Table 1](#)), split for cases when the NuWro INC is and is not applied.

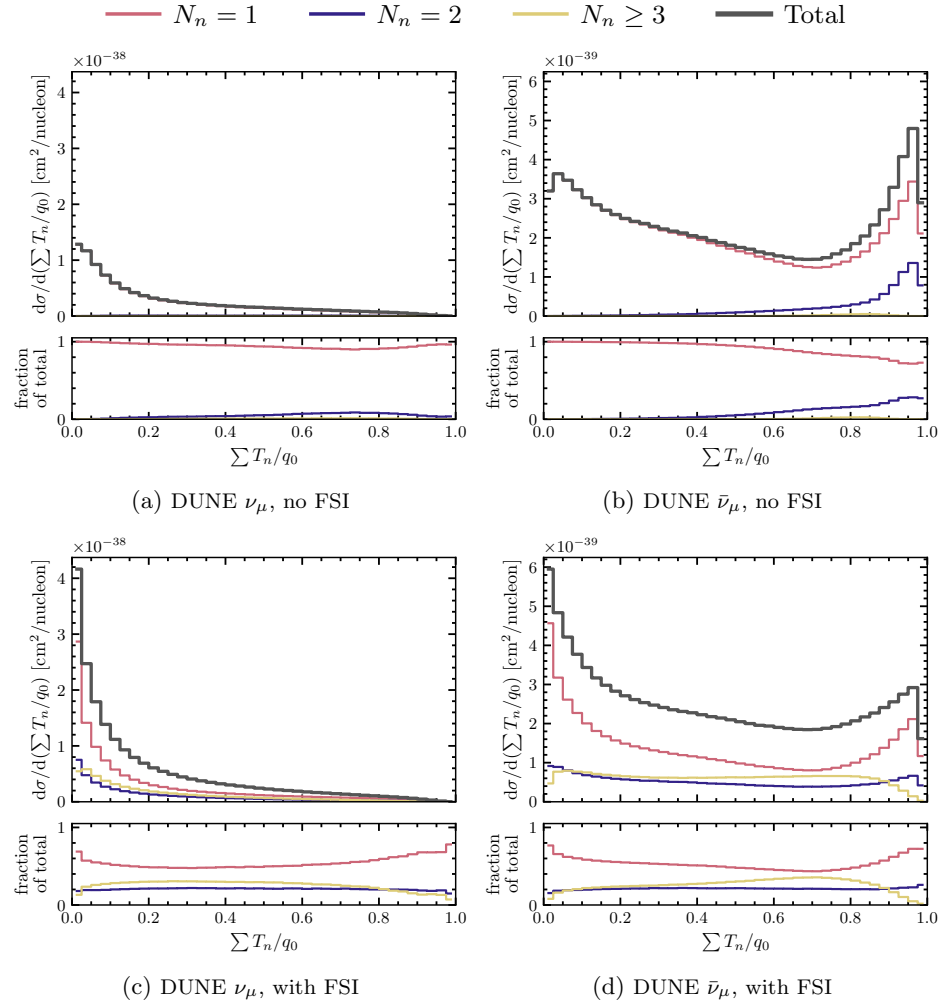


Figure 8: The NuWro simulated distribution of the ratio between the sum of final-state neutron kinetic energies (ΣT_n) and the interaction energy transfer (q_0) for CC inclusive ν_μ or $\bar{\nu}_\mu$ interactions on an argon target at the DUNE FD using the oscillated DUNE flux (see Table 1). The distribution is split by the number of final state neutrons (N_n) in the simulated interactions.

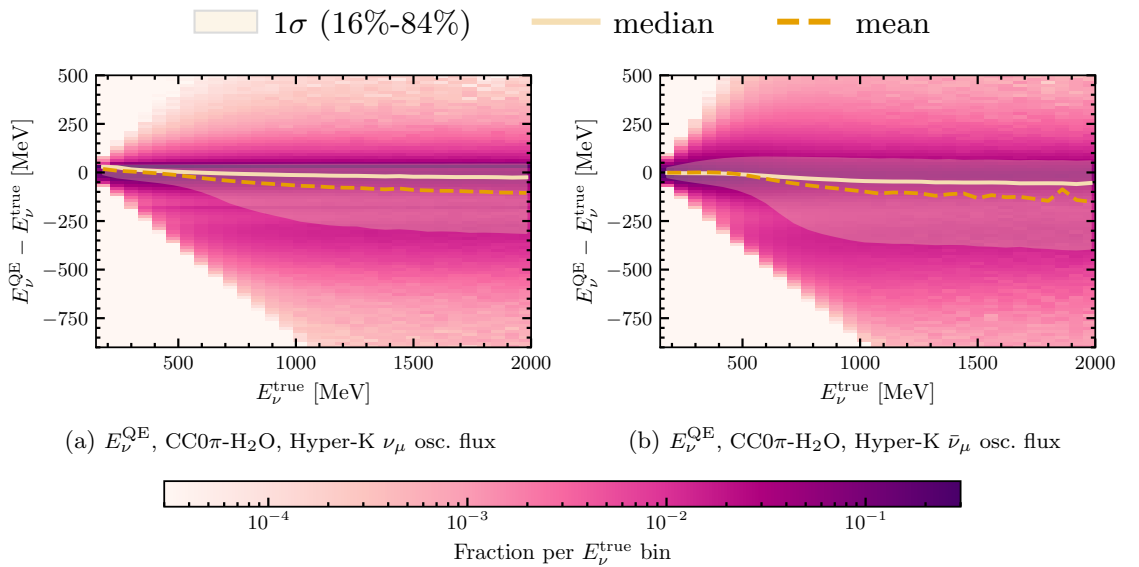


Figure 9: The NuWro simulated neutrino energy estimation bias shape (using E_ν^{QE}) for CC0 π ν_μ or $\bar{\nu}_\mu$ interactions on a water target as a function of true neutrino energy. The mean, median and a band containing 16-84% of the bias are shown.

4.4 FSI model variations

Figure 6 and Figure 7 demonstrate large differences in neutrino energy estimation bias between cases where FSI (or some aspect of it) is or is not modelled. This is an overly conservative modification, as the need for FSI is well established. Here we consider a number of more realistic variations of FSI modelling, and quantify the impact each has on neutrino energy estimation bias, covering:

- Variations of the pion absorption probability within the NuWro INC. We performed a minimal change to the NuWro source code by introducing a single parameter which directly scales the pion absorption cross section used in the INC. Prior attempts to tune INC models to pion-scattering measurements [77] suggest significant uncertainty on the probability for pion absorption. Based on the prescription in Refs.[77, 78] we vary the pion absorption interaction cross section within the NuWro INC by $\pm 31\%$. A change of a similar size is prescribed by findings in Ref. [29].
- Variations of the nucleon interaction probability inside the NuWro INC. Based on uncertainties in measurements of nucleon transparency from electron scattering [79, 80], we consider variations of the nominal NuWro simulation in which the mean free path (MFP) between interactions of nucleons within the INC is varied by $\pm 30\%$ using existing NuWro parameters.
- Variations of the entire INC model used. Different INCs make different assumptions regarding propagation of hadrons, the kinematics of scatters and the role of nuclear effects, and tune the relative importance of processes using different data sets. We vary the INC considered among the four models available within GENIE discussed in section 2. The impact of the variation of these models on DUNE neutrino energy reconstruction is also discussed in Ref. [11].

In the cases where we vary the pion absorption probability and the nucleon mean free path, the size of the variation is extracted from measurements on light nuclei such as carbon and oxygen. For the purpose of this work we apply the same variation for interactions on an argon target. Future analyses, for example exploiting recent measurements of pion-argon and proton-argon scattering such as Ref. [81, 82, 83], may provide different ranges for varying these parameters in future studies.

Figure 12, Figure 13, and Figure 14 show the difference between the true neutrino energy and each neutrino energy estimator for each of the three FSI model variations. For easier comparison between the Hyper-K and DUNE cases, the neutrino energy estimation bias *relative* to the true neutrino energy is shown. Similar figures considering the impact of simply turning FSI on and off are shown in Appendix B. For the DUNE and Hyper-K neutrino and antineutrino cases, the figures illustrate how the mean, median and spread of the neutrino energy estimation bias changes for each variation.

The change in the mean and median estimation bias for each variation is summarised in Table 2, and the same shifts expressed relative to the true neutrino energy are provided in Appendix C. Whilst variations of the mean are most indicative of an energy estimation scale shift comparable with the ~ 5 MeV and ~ 15 MeV requirements for ultimate precision in section 3, a comparison of the mean and median helps to show how the energy estimation bias is reshaped by FSI as well as shifted on average. The table also includes the impact of turning FSI on and off as well as the impact of applying a nuclear potential (as described in subsection 4.3). For the latter, note that only ν_μ CCQE interactions are simulated.

Since pion absorption is the dominant driver of neutrino energy estimation bias from INC FSI for Hyper-K, varying its strength almost directly varies the size of the FSI/no-FSI differences shown in Figure 6. For DUNE the impact is less pronounced. Whilst the absorption of pions moves events between the discrete pion peaks shown in Figure 7a, it also redistributes some of the absorbed pion kinetic energy to outgoing neutrons.

Varying the nucleon MFP has very little impact on Hyper-K neutrino energy estimation, as outgoing nucleons are not measured. The only effect is to marginally alter the small probability for pion production within the INC, migrating some CCQE interactions out of the $CC0\pi$ sample of interactions considered. For DUNE, a smaller (larger) MFP nucleon increases (decreases) the probability for protons to transfer energy to neutrons. For neutrino interactions, which produce more protons than neutrons at the interaction vertex, the impact of a lower MFP is therefore to redistribute energy from protons to neutrons, increasing the neutrino energy estimation bias. For antineutrino interactions, which contain more neutrons than protons, the effect is the opposite.

Alterations to the INC model itself implicitly change both the pion absorption probability and the nucleon MFP at the same time as varying the kinematics of each process in the INC (e.g. the

amount of momentum transferred to protons or neutrons in a typical pion absorption). Since Hyper-K is predominantly sensitive to only the probability of pion absorption (and not the kinematics of the process), and the INCs all have similar pion absorption probabilities (likely from tuning to similar pion scattering data sets), the impact on Hyper-K neutrino energy estimation is smaller than for DUNE. It is not negligible, however: the median bias shifts by less than 1 MeV, but the mean shifts by up to ~ 9 MeV. Because each pion-absorption event carries a large bias (~ 250 – 500 MeV, [Figure 6](#)), even small differences in pion absorption probability between the INC models move the mean of the bias distribution while leaving its median almost unchanged. For DUNE, altering the INC can change the fraction of energy carried away by neutrons or the pion multiplicity in complicated ways, leading to a significant impact on the neutrino energy estimation bias. The INC variations affect the DUNE-case neutrino and antineutrino energy estimators similarly.

Flavour	Observable	FSI / no FSI		$\pi_{\text{abs}} \pm 31\%$		NN MFP $\pm 30\%$		INC model var.		Nuc. Pot. on/off	
		median [MeV]	mean [MeV]	median [MeV]	mean [MeV]	median [MeV]	mean [MeV]	median [MeV]	mean [MeV]	median [MeV]	mean [MeV]
ν_μ	Hyper-K E_ν^{QE}	10.1	35.8	5.8	16.4	0.2	1.0	0.8	9.4	7.0	4.4
	DUNE E_ν^{avail}	28.7	79.4	1.6	2.9	10.6	4.2	44.5	32.2	0.3	4.5
	DUNE E_ν^{had}	88.7	81.9	13.8	10.7	16.3	2.4	39.2	27.1	0.3	4.1
$\bar{\nu}_\mu$	Hyper-K E_ν^{QE}	7.0	25.6	3.6	12.5	0.3	1.1	0.1	2.0		
	DUNE E_ν^{avail}	39.8	35.4	7.7	6.5	14.7	16.2	39.8	16.4		
	DUNE E_ν^{had}	55.1	43.0	17.8	13.7	17.3	18.7	61.7	37.0		

Table 2: The maximum shift in the mean and median neutrino energy estimation bias due to different FSI variations for the Hyper-K and DUNE neutrino and antineutrino cases. The numbers reported for the INC model variation is derived from the two INC models that give the largest spread in the mean. Red boxes indicate that the variation is larger than 5 MeV or 15 MeV for the Hyper-K and DUNE cases respectively, which is broadly indicative of how well the neutrino energy reconstruction scale must be controlled (see [section 3](#)). “Nuc. Pot.” stands for the nuclear potential considered in [subsection 4.3](#), for which the table reports a shift derived considering only CCQE interactions.

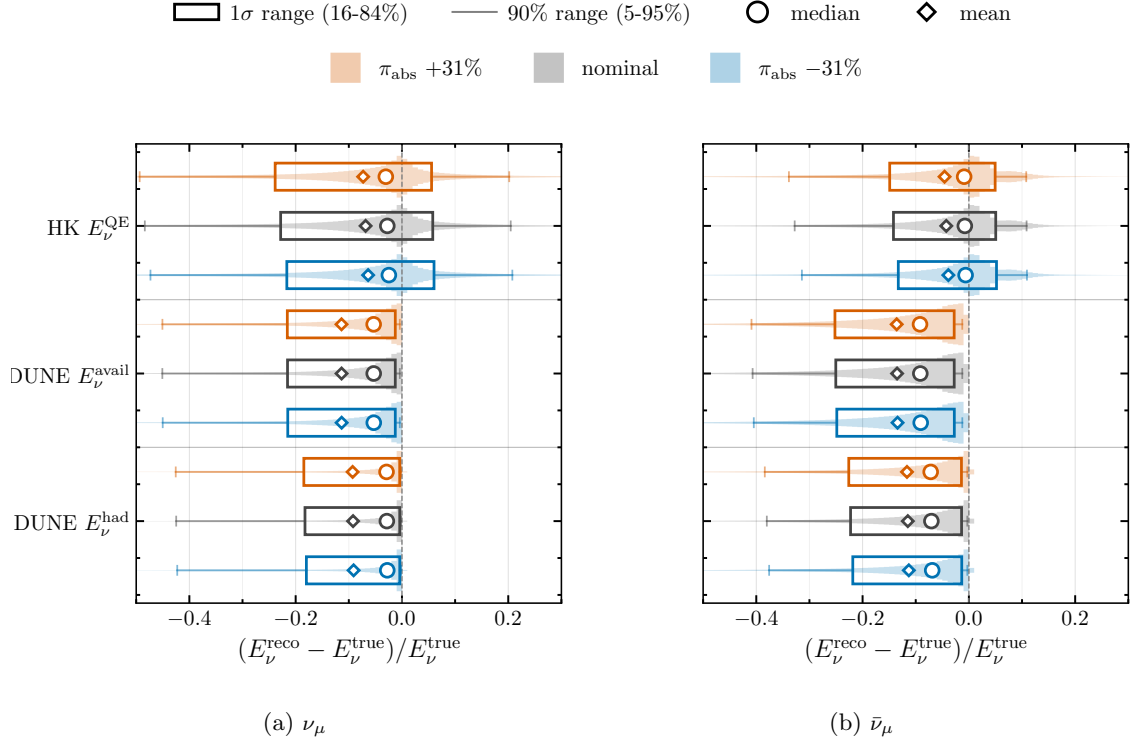


Figure 12: The relative neutrino energy estimation bias, $(E_\nu^{\text{reco}} - E_\nu^{\text{true}})/E_\nu^{\text{true}}$, for the Hyper-K case (where $E_\nu^{\text{reco}} = E_\nu^{\text{QE}}$), and DUNE cases (where $E_\nu^{\text{reco}} = E_\nu^{\text{avail}}$ or $E_\nu^{\text{reco}} = E_\nu^{\text{had}}$), for NuWro simulations with the pion absorption probability modified by $\pm 31\%$. The silhouette shows the shape of the energy estimation bias, overlaid with the median (open circle) and mean (open diamond) bias, as well as a box giving the 1σ (16-84%) range of the distribution and faint 90% whiskers (5-95%).

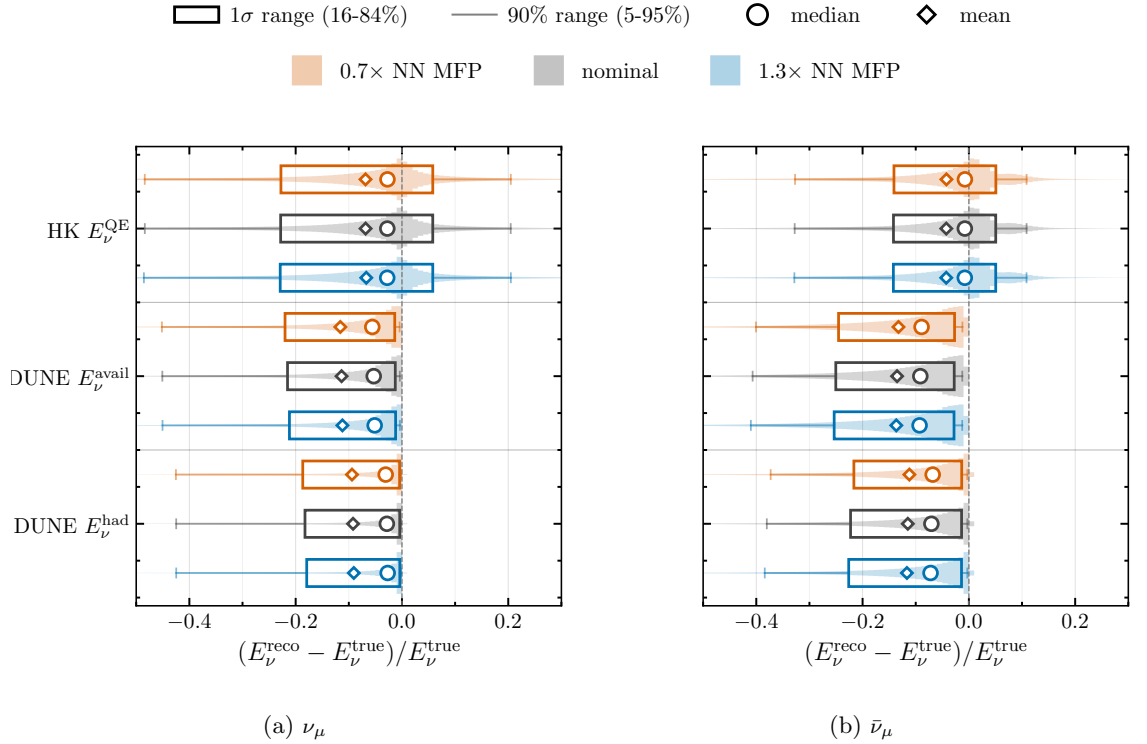


Figure 13: The same as Fig. 12 but considering $\pm 30\%$ alterations to the nucleon MFP within the INC.

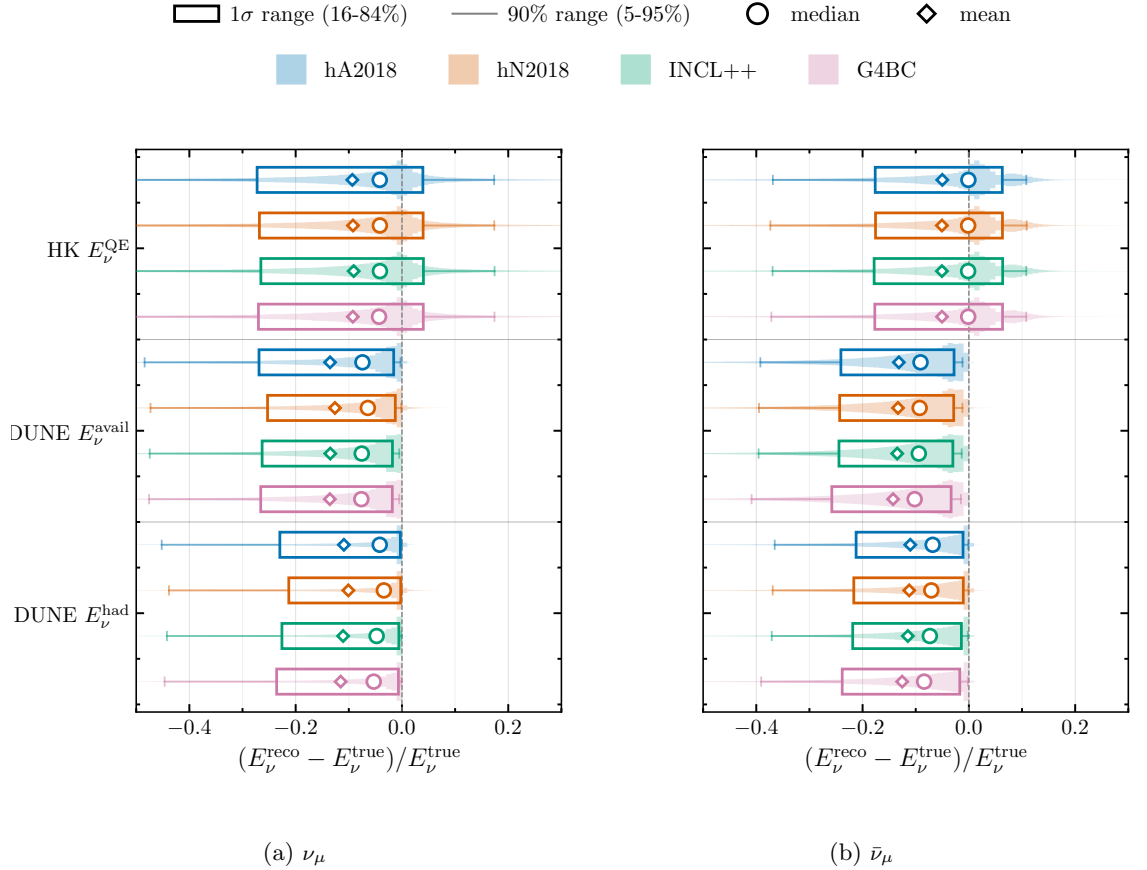


Figure 14: The same as Fig. 12 but considering four GENIE INC model variations.

5 Discussion

The analysis presented in [section 4](#) clearly demonstrates that FSI has the potential to be an important driver of neutrino energy estimation bias for both DUNE and Hyper-K. Several of the realistic variations of FSI models cause shifts in the median and mean estimation bias significantly exceeding the ~ 5 MeV and ~ 15 MeV precision requirements. Beyond this overall conclusion, the results also reveal that FSI affects the two experiments in fundamentally different ways that follow directly from the differences in the experiments' energy estimators.

The Hyper-K E_ν^{QE} estimator is built from lepton kinematics alone and is therefore blind to any INC effect that does not change the probability for a neutrino interaction to leave a $\text{CC}0\pi$ topology. As discussed in [subsection 4.2](#), the only INC effect that significantly biases E_ν^{QE} is pion absorption, which moves resonant pion production events, for which [Equation 3](#) produces a bias, into the $\text{CC}0\pi$ topology. Conversely, INC-driven changes to nucleon kinematics or charged pion multiplicities above zero are invisible to the Hyper-K energy estimator. The DUNE E_ν^{had} estimator behaves in the opposite way: it is largely insensitive to topology migrations of the $\text{CC}0\pi/\text{CC}1\pi$ type but is strongly affected by any aspect of FSI that alters the fraction of the hadronic energy carried by neutrons. This leaves the estimator particularly sensitive to variations of the different GENIE INC models, whilst showing more modest sensitivity to variations of the nucleon MFP and pion absorption (the latter being more impacted by energy transferred to neutrons during the absorption process than because of the absorption itself). The DUNE E_ν^{avail} estimator is additionally sensitive to the multiplicity of charged pions. Interestingly, at least for the NuWro INC, this actually reduces its sensitivity to changes in pion absorption. This is because the absorption of a pion reduces bias which actually counteracts the increase in bias from any potential kinetic energy transferred to neutrons during the absorption.

The results in [subsection 4.3](#) demonstrate that FSI effects beyond those considered in an INC are important, especially for Hyper-K. Whilst incorporating the nuclear mean-field potential causes a small shift in the mean of the E_ν^{QE} bias distribution for CCQE interactions, the distribution is significantly reshaped, as shown by the ~ 7 MeV median shift and [Figure 11](#). For DUNE, the role of the nuclear potential in CCQE interactions seems less pronounced. However, an analogous microscopic treatment for pion production could in principle have a more direct impact on

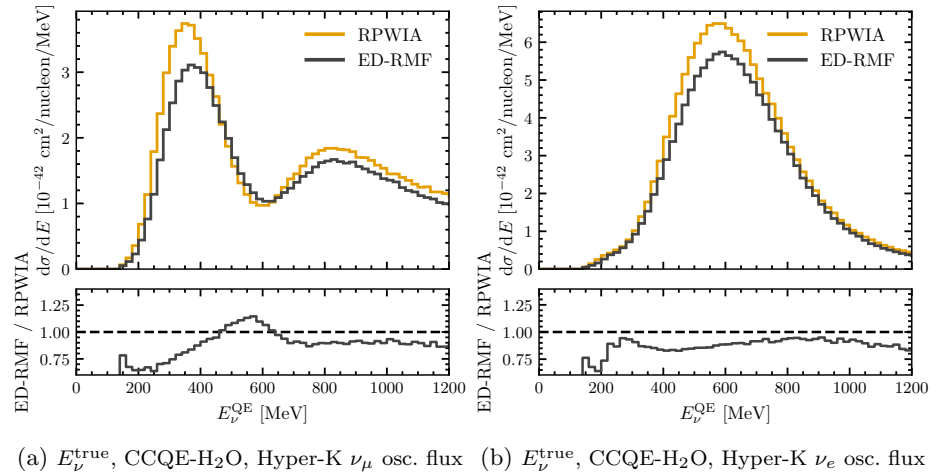


Figure 15: The NEUT simulated rate of CCQE ν_μ or ν_e interactions on water using the oscillated Hyper-K flux (see Table 1) as a function of estimated neutrino energy (E_ν^{QE}) using the ED-RMF and RPWIA models.

calorimetric estimators, and quantifying this remains an open challenge.

A further feature of the variations summarised in Table 2 is that FSI modelling does not generally affect neutrino and antineutrino energy estimation symmetrically. In particular, the nucleon MFP variations for DUNE cause shifts in the opposite direction for neutrinos and antineutrinos. Moreover, shifts from INC model variations can reshape the energy estimation bias for the DUNE estimators quite differently for neutrinos and antineutrinos, as seen by the different impact on the bias medians. The implication for oscillation analyses may be significant, since sensitivity of δ_{CP} is at least partially extracted from differences between the oscillated neutrino and antineutrino spectra, which may thus be confused by FSI mismodelling.

Importantly, Figure 9 and Figure 10 show that neutrino energy estimation biases introduced by FSI are not constant in neutrino energy. The figure demonstrates that both kinematic and calorimetric biases grow with E_ν , driven for Hyper-K by the rising contribution of CCnph and pion production relative to CCQE above ~ 0.5 GeV, and for DUNE by the increasing typical energy transfer and the associated growth in neutron emission and charged-pion multiplicity. This energy dependence has an important implication for the use of ND measurements to constrain the size of the bias. The ND and FD see different neutrino energy spectra (since the latter is shaped by oscillations), the FSI-driven bias does not compensate between the two detectors, and an ND constraint on the bias necessarily relies on the underlying interaction model to extrapolate across energies. However, this may be partially mitigated through use of movable ND and the PRISM technique [84, 16, 85].

The richness of the FSI-related effects on neutrino energy estimation is difficult to capture with simple summary metrics, such as the mean and median reported in Table 2. Figure 15 illustrates this for the change of nuclear potential in NEUT (the difference between ED-RMF and RPWIA). Although this variation yields a negligible shift in the mean according to Table 2, it produces a much larger median shift and substantially reshapes the CCQE component of the spectrum. This disparity between the mean and median shifts is a direct consequence of the asymmetric way the nuclear potential reshapes the distribution.

Throughout this work, we have primarily considered the bias in the neutrino energy estimators averaged over the oscillated ν_μ or $\bar{\nu}_\mu$ energy spectra. However, the appearance spectra for ν_e and $\bar{\nu}_e$ have a significantly different shape than the ν_μ and $\bar{\nu}_\mu$ spectra, as shown in Figure 1 and discussed in subsection 3.3. Since the bias itself varies with neutrino energy, as demonstrated in Figure 9 and Figure 10, this different spectral shape leads to a different flux-averaged result. In addition, although the way that ν_μ and ν_e cross sections differ is well known and (assuming lepton universality) driven only by the lepton mass, the flux-averaged ν_e and ν_μ event rates remain susceptible to uncertainties in how poorly understood nuclear effects convolve with the available interaction phase space, which differs between the two species [86, 87, 88, 89]. We have nevertheless checked that the observations made for ν_μ and $\bar{\nu}_\mu$ interactions remain similar in the ν_e and $\bar{\nu}_e$ case. The most notable difference is that the DUNE INC model spread increases slightly for both neutrinos and antineutrinos. The scale of the mean and median variations due to FSI modelling remains similar to that presented in Table 2 and the discussion based on the ν_μ and $\bar{\nu}_\mu$

flux-averaged results is representative for the case of ν_e and $\bar{\nu}_e$ appearance.

Overall, the results of [section 4](#) clearly demonstrate the importance of FSI modelling for DUNE and Hyper-K, but the shifts presented in [Table 2](#) should not be read as quantitatively indicative of systematic uncertainties that the experiments will face. Firstly, the variations shown are raw model spreads, presented without any constraint from ND measurements. In a real oscillation analysis, FSI parameters would be treated as nuisance parameters and constrained through fits to ND data, so that the residual bias propagated to the FD would be substantially smaller than the raw spread. The power of ND constraints will depend on detector performance and the development of a neutrino interaction model, and associated uncertainties, that can describe the ND data. Secondly, we have considered the impact of FSI on neutrino energy estimation in isolation from other observables. In practice, FD measurements can be binned in additional kinematic variables beyond estimated neutrino energy (for example visible hadronic energy, or observed proton and pion multiplicities), which can provide additional handles to disentangle FSI-driven migrations from genuine oscillation effects. The extent to which such multi-dimensional analyses can mitigate the biases shown here is a question we do not address in this work. Thirdly, how these energy-estimation shifts ultimately translate into biases on the measured oscillation parameters is impossible to assess quantitatively without a full oscillation analysis. As [Figure 15](#) shows, even a variation with a negligible mean shift can move the oscillation dip (by ~ 18 MeV for the nuclear-potential change) and alter the normalisation of the oscillated spectra (unlike the INC variations, which are designed to conserve the inclusive cross section as a function of lepton kinematics). In summary, [Table 2](#) should be read as characterising the size of the FSI modelling problem to be solved and not the size of the residual bias entering a final oscillation analysis.

There are some clear opportunities to confront the challenges in FSI modelling faced by next generation neutrino oscillation experiments. For Hyper-K, a key priority is to ensure that pion absorption on oxygen is well modelled and is accompanied by robust uncertainties that can be constrained at the ND. This would be greatly facilitated by new pion-oxygen scattering measurements to supplement the limited available data at relevant kinematics for Hyper-K [\[77\]](#), which could be used to directly benchmark INC models. In parallel, microscopic FSI treatments must also be accompanied by uncertainties to allow an ND constraint and ideally extended beyond CCQE so that the ED-RMF-type shifts seen in this work can be assessed for the CCnph and pion-production channels. For DUNE, the priority is to constrain the repartition of hadronic energy between neutrons, protons and pions caused by FSI. New proton- and pion-argon scattering measurements from ProtoDUNE, building on its existing results [\[83, 82\]](#), may provide an important constraint, especially if the energy transferred to neutrons can be inferred through exclusive, differential analyses. Moreover, with high precision detectors and large projected statistics, measurements from the DUNE ND [\[16\]](#) itself will be well placed to constrain FSI modelling, provided sufficient work has been done to develop a parameterised neutrino interaction model that can be constrained. In both the DUNE and Hyper-K cases, the path to controlling FSI at the level to allow the experiments to reach their ultimate sensitivity requires coupling theoretical developments to a dedicated programme of experimental measurements.

6 Conclusions

In this work, we have used state-of-the-art neutrino interaction event generators to characterise the impact of FSI modelling on the neutrino energy estimators that DUNE and Hyper-K will use to extract oscillation parameters, considering both the semi-classical INC that dominate current simulations and a microscopic treatment based on a relativistic nuclear potential. We have shown that the target precisions on oscillation parameter measurements quoted by Hyper-K and DUNE correspond broadly to a control of the estimated neutrino energy scale at the level of ~ 5 MeV and ~ 15 MeV respectively. Realistic variations of FSI models produce shifts in neutrino energy estimation bias that are at or above these target energy scale precisions. The two experiments are sensitive to different FSI physics: the kinematic estimator used at Hyper-K is driven primarily by the probability of pion absorption and by the consideration of a mean-field nuclear potential outside the semi-classical INC paradigm; the calorimetric estimators used at DUNE are driven by the distribution of hadronic energy between neutrons, protons and pions.

The variations reported here should be understood as characterising the size of the FSI modelling problem to be solved, rather than as residual systematic uncertainties on an oscillation analysis, which will benefit from ND constraints. The path to controlling FSI at the level demanded by DUNE and Hyper-K requires coordinated progress on two fronts: continued theoretical development of FSI models, including the extension of microscopic treatments to channels beyond CCQE and the construction of robust parameterised uncertainties that can be

propagated through oscillation analyses; and a dedicated programme of experimental measurements targeted at the specific aspects of FSI to which each experiment is most sensitive.

Acknowledgments

The authors thank R. Dharmapal Banerjee for help with the NuWro event generator, C. Wilkinson for having produced the GENIE simulation files used for this work and L. Pickering for providing software containers including NUISANCE and neutrino event generators used in early iterations of this work. J. McKean was supported by Grant-in-Aid for JSPS Research Fellows, JSPS KAKENHI Grant No. 25KF0223.

A Impact of the neutrino energy estimation bias on antineutrino oscillation spectra

In this appendix, we perform an analogous study to the one presented in [subsection 3.3](#), but where we focus on the impact of oscillations and energy scale changes on *antineutrino* FD spectra.

[Figure 16](#) shows that the impact of oscillation parameter variations and energy scale shifts is similar in shape and magnitude to the cases discussed in [Figure 2](#). The energy scale variations for antineutrinos are slightly larger than a variation of 0.4% on Δm_{32}^2 and retain the same shape as in the neutrino case. For $\bar{\nu}_e$ appearance, the energy scale variations are slightly smaller than the δ_{CP} variation but remain comparable.

[Figure 17](#) shows the same variations as in [subsection 3.3](#) applied to the DUNE antineutrino spectrum. For the $\bar{\nu}_\mu$ disappearance, the energy scale shift is comparable in both shape and magnitude to the shift in Δm_{32}^2 , like in the neutrino case. However, the $\bar{\nu}_e$ appearance spectrum shows a significant difference with respect to the neutrino case. As discussed in [subsection 3.3](#), a shift in δ_{CP} acts as a shape effect, with a response $\partial P/\partial\delta_{\text{CP}} \propto -\sin(\Delta m_{32}^2 L/4E + \delta_{\text{CP}})$ that is, in vacuum, of similar size for ν_e and $\bar{\nu}_e$. What governs the visible distortion, however, is the size of this response *relative* to the appearance probability $P(\nu_\mu \rightarrow \nu_e)$ itself. This probability is dominated by a δ_{CP} -independent term whose size is set by the mixing angles, $\propto \sin^2\theta_{23}\sin^2 2\theta_{13}$; the δ_{CP} -carrying interference term sits on top of it as a smaller modulation, suppressed by the ratio of the mass splittings $\alpha = \Delta m_{21}^2/\Delta m_{31}^2 \approx 0.03$. Matter effects act on the dominant term with opposite sign for neutrinos and antineutrinos, enhancing it for ν_e and suppressing it for $\bar{\nu}_e$. A given δ_{CP} shift therefore distorts the ν_e probability by a smaller relative amount and the $\bar{\nu}_e$ probability by a larger one. Consequently, for $\bar{\nu}_e$ the distortion from a δ_{CP} variation is both larger than, and different in shape from, that produced by a 15 MeV energy-scale shift, whereas for ν_e the two are comparable. For Hyper-K, the much shorter baseline renders matter effects less pronounced, so this asymmetry between ν_e and $\bar{\nu}_e$ does not appear significant.

In a real oscillation analysis, all samples are fitted simultaneously and so correlations between them, which the isolated single-sample spectra shown so far do not capture, are exploited to constrain the oscillation parameters. To investigate the impact of considering multiple oscillation samples in one simple way, we compare how energy scale shifts and δ_{CP} change the ratio of the ν_e to $\bar{\nu}_e$ event rates⁹. [Figure 18](#) and [Figure 19](#) show that, for both the Hyper-K and DUNE cases, variations of δ_{CP} around its nominal value of $-\pi/2$ distort this ratio in a way that differs in shape from, and is larger in magnitude than, the distortion induced by an energy-scale shift at the levels considered in this work. This demonstrates how the consideration of neutrino and antineutrino samples simultaneously can help reduce the impact of neutrino energy estimation bias on δ_{CP} determination. We stress, however, that this does not imply that FSI or energy-scale effects are unimportant; it reflects only that, within the standard three-flavour PMNS framework and at the energy-scale precision considered here, their impact on the $\nu_e/\bar{\nu}_e$ ratio is subdominant to that of δ_{CP} . Searches for physics beyond this paradigm, such as non-standard interactions, may alter the ν_e and $\bar{\nu}_e$ spectra in ways that are degenerate with energy-scale changes, and so may require the neutrino energy scale to be controlled at a different, potentially more stringent, level than the one considered here.

⁹Note that the experiments plan to run with significantly different relative neutrino and antineutrino exposures (1:1 for DUNE and 1:3 for Hyper-K) and so a comparison of absolute value of the ratio between them is not meaningful

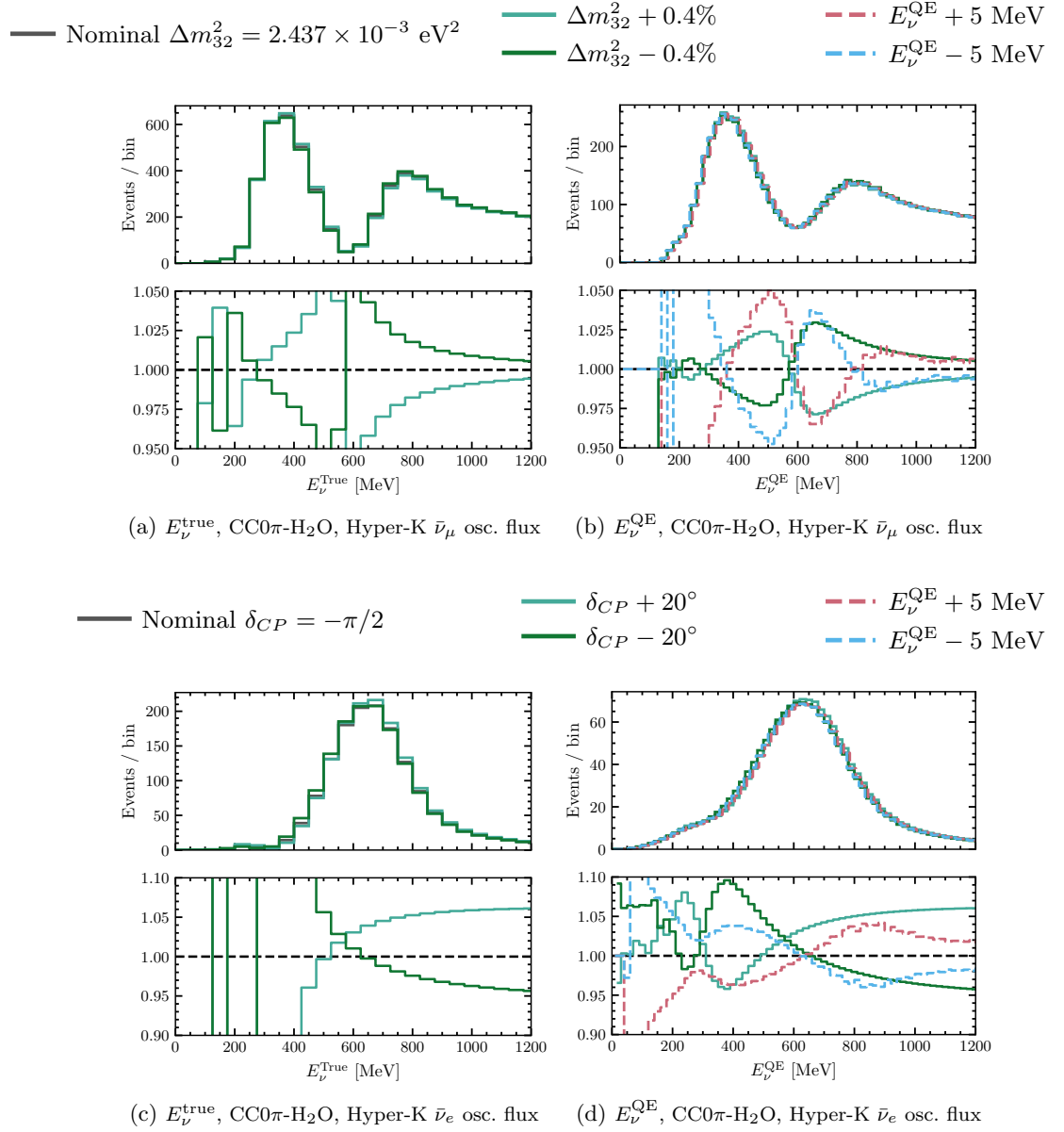


Figure 16: The NuWro simulated rate of CC0 π $\bar{\nu}_\mu$ or $\bar{\nu}_e$ interactions on water at the Hyper-K FD using the oscillated Hyper-K flux (see Table 1) as a function of true (E_ν^{true}) or estimated (E_ν^{QE}) neutrino energy. For the former, variations of oscillation parameters corresponding to the Hyper-K ultimate target precision are shown. For the latter, these are compared to E_ν^{QE} biased by ± 5 MeV.

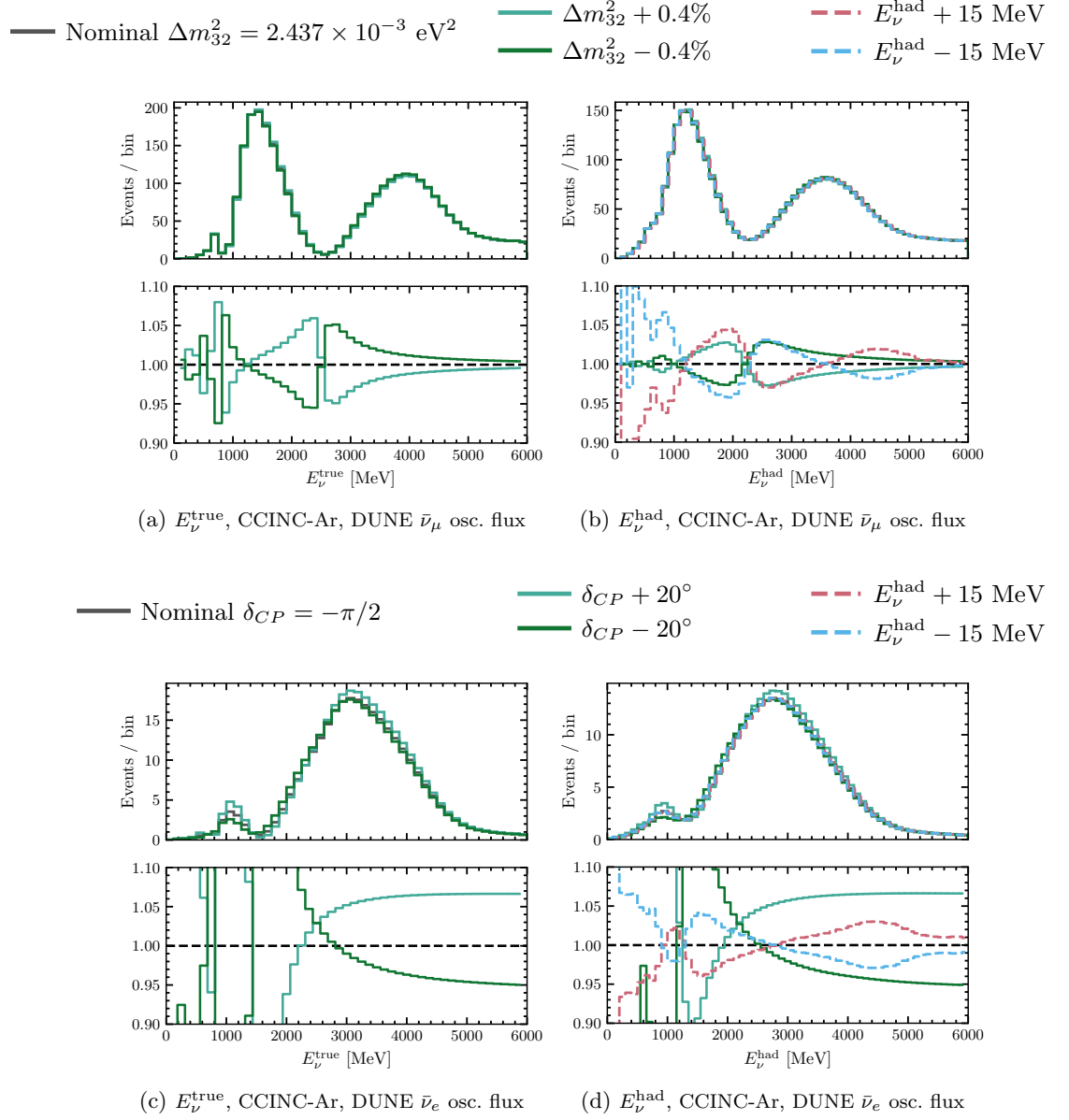


Figure 17: The NuWro simulated rate of CC inclusive $\bar{\nu}_\mu$ or $\bar{\nu}_e$ interactions on argon at the DUNE FD using the oscillated DUNE flux (see Table 1) as a function of true (E_ν^{true}) or estimated (E_ν^{had}) neutrino energy. For the former, variations of oscillation parameters corresponding to the DUNE ultimate target precision are shown. For the latter, these are compared to E_ν^{had} biased by $\pm 15 \text{ MeV}$.

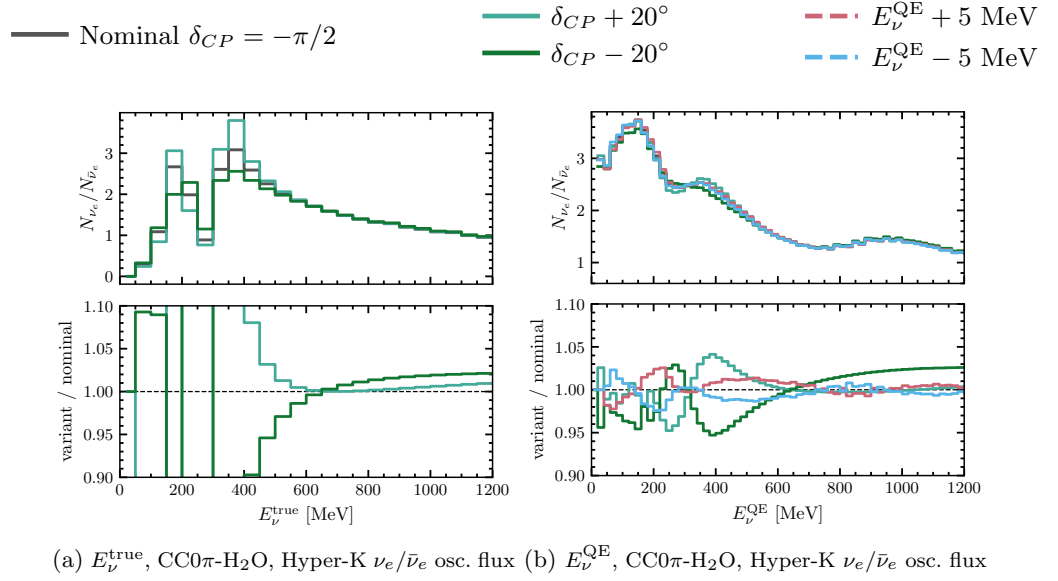


Figure 18: The ratio of NuWro simulated rate of CC0 π ν_e to $\bar{\nu}_e$ interactions on water at the Hyper-K FD using the oscillated Hyper-K flux (see Table 1) as a function of true (E_{ν}^{true}) or estimated (E_{ν}^{QE}) neutrino energy. For the former, variations of oscillation parameters corresponding to the Hyper-K ultimate target precision are shown. For the latter, these are compared to E_{ν}^{QE} biased by ± 5 MeV.

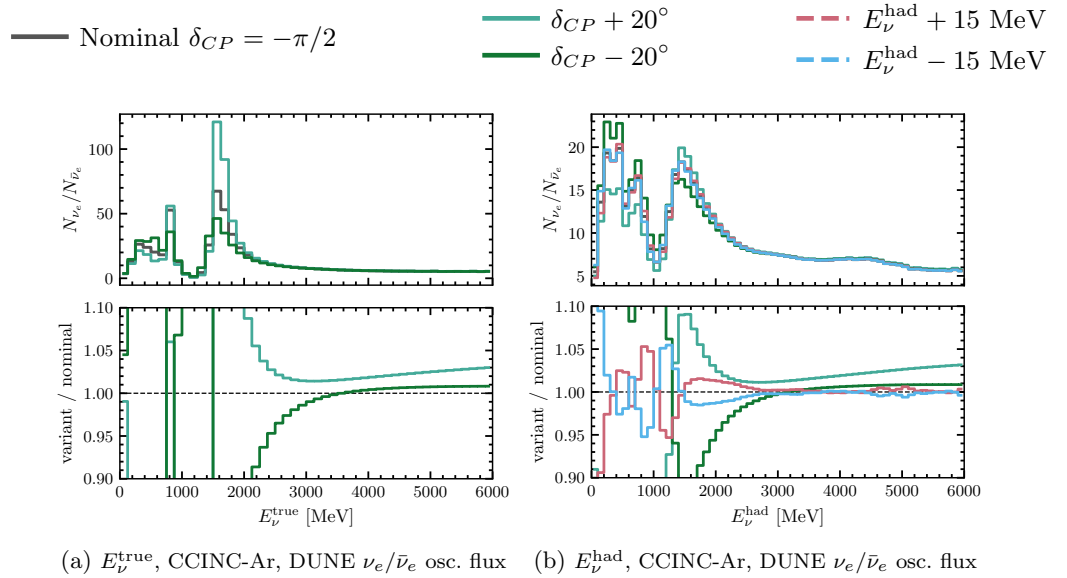


Figure 19: The ratio of NuWro simulated rate of CC inclusive ν_e to $\bar{\nu}_e$ interactions on argon at the DUNE FD using the oscillated DUNE flux (see Table 1) as a function of true (E_{ν}^{true}) or estimated (E_{ν}^{had}) neutrino energy. For the former, variations of oscillation parameters corresponding to the DUNE ultimate target precision are shown. For the latter, these are compared to E_{ν}^{had} biased by ± 15 MeV.

B Additional figures for FSI on/off variations

Figure 20 and Figure 21 summarise the impact of turning on and off the INC and the nuclear potential on the performance of the neutrino energy estimators considered in this work, supplementing the specific FSI variations considered in Figure 12, Figure 13 and Figure 14.

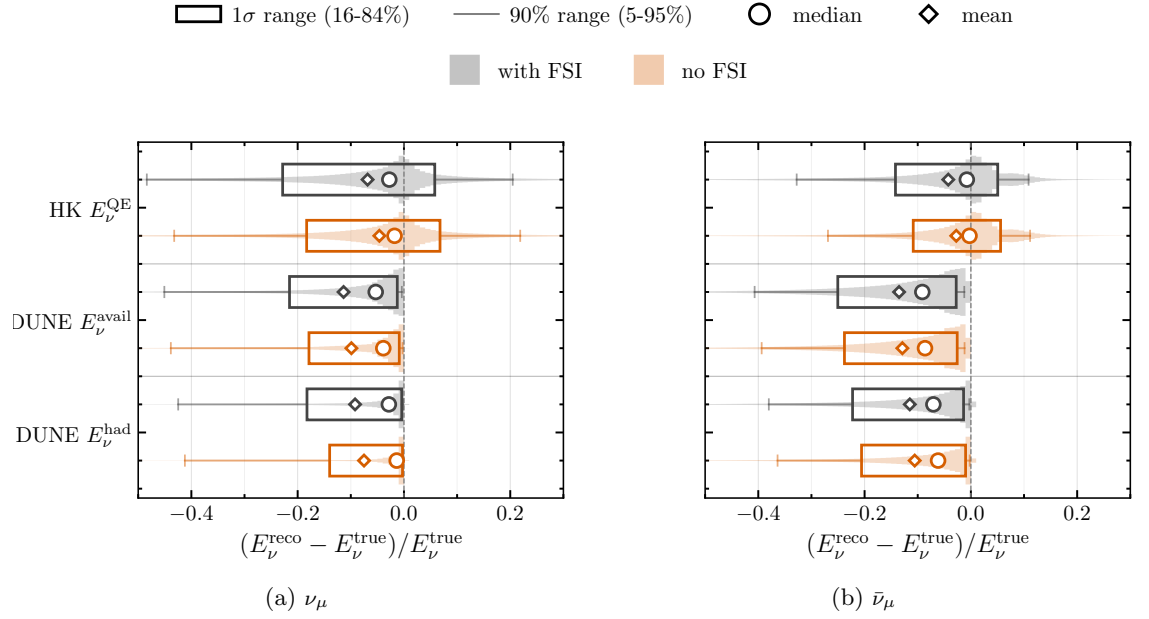


Figure 20: The same as Fig. 12, comparing the effect of turning on and off the INC within NuWro.

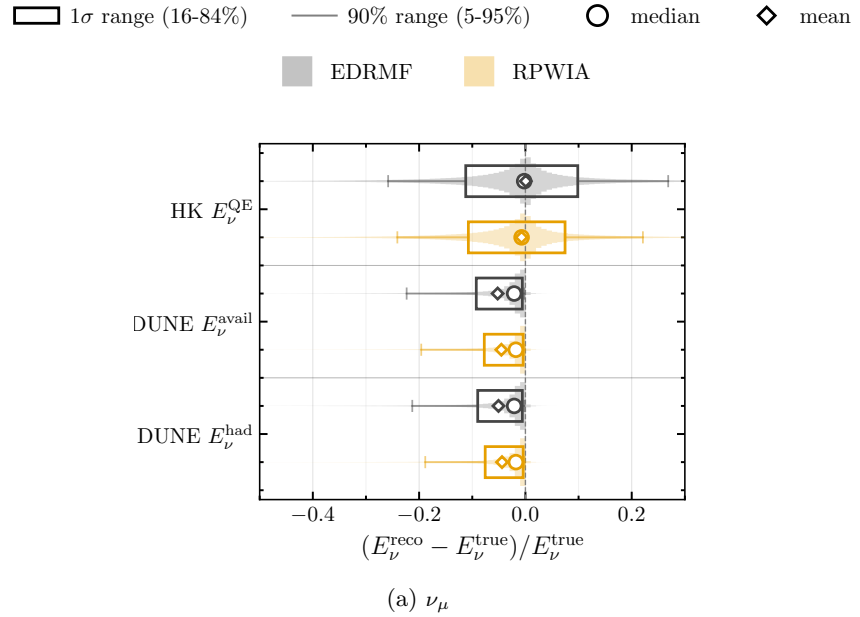


Figure 21: The same as Fig. 12, comparing the NEUT ED-RMF and RPWIA nuclear models for CCQE interactions only.

C Relative bias studies

In Table 2 the sensitivity to the energy-estimation bias to FSI model variations is quantified in *absolute* terms (as the difference between the estimated and true neutrino energy in MeV). Since Hyper-K and DUNE operate at substantially different mean neutrino energies, it is also informative to express the bias *relative* to the true neutrino energy, $(E_\nu^{\text{reco}} - E_\nu^{\text{true}})/E_\nu^{\text{true}}$, which places the two experiments on a more common footing. Table 3 reproduces the absolute shifts of Table 2 whilst

also reporting their relative counterparts. We recall that the ~ 5 MeV (Hyper-K) and ~ 15 MeV (DUNE) absolute targets broadly correspond to a shift of $\sim 0.5\%$ of the respective mean neutrino energy (see [subsection 3.3](#)); the 0.5% threshold used to flag the relative shifts is therefore the common relative counterpart of these two absolute requirements. We note, however, that the absolute and relative measures are not equivalent: normalising by E_ν^{true} gives proportionally less weight to high-energy interactions, where the absolute bias is largest, so the two measures provide a slightly different quantification of the change in energy estimation bias.

Overall, [Table 3](#) shows that the main conclusions of [section 4](#) are preserved when considering relative bias shifts, although several details differ in instructive ways. For the DUNE case, varying the full INC model remains the dominant effect. The pion-absorption variation, which reaches the 15 MeV scale for E_ν^{had} in absolute terms, becomes a much smaller effect in relative terms. The relative sensitivity to the nucleon mean free path (MFP) is also reduced but remains significant for antineutrinos, where it skews the bias distribution. For the Hyper-K case, the dominant effects are the pion absorption probability and FSI beyond the semi-classical INC. In particular, the relative shift in the mean bias between the ED-RMF and RPWIA models now exceeds the 0.5% threshold, whereas the corresponding absolute shift lies below the 5 MeV threshold. This further highlights the importance of FSI modelling beyond the cascade picture for Hyper-K. A comparable relative shift from the ED-RMF/RPWIA comparison is also seen for DUNE. We recall, however, that it is computed for CCQE interactions only, which make up less than one third of the DUNE event rate, so this particular conclusion is harder to generalise.

Flavour	Observable	FSI / no FSI		$\pi_{\text{abs}} \pm 31\%$		NN MFP $\pm 30\%$		INC model var.		Nuc. Pot. on/off	
		median	mean	median	mean	median	mean	median	mean	median	mean
Absolute bias [MeV]											
ν_μ	Hyper-K E_ν^{QE}	10.1	35.8	5.8	16.4	0.2	1.0	0.8	9.4	7.0	4.4
	DUNE E_ν^{avail}	28.7	79.4	1.6	2.9	10.6	4.2	44.5	32.2	0.3	4.5
	DUNE E_ν^{had}	88.7	81.9	13.8	10.7	16.3	2.4	39.2	27.1	0.3	4.1
$\bar{\nu}_\mu$	Hyper-K E_ν^{QE}	7.0	25.6	3.6	12.5	0.3	1.1	0.1	2.0		
	DUNE E_ν^{avail}	39.8	35.4	7.7	6.5	14.7	16.2	39.8	16.4		
	DUNE E_ν^{had}	55.1	43.0	17.8	13.7	17.3	18.7	61.7	37.0		
Relative bias [%]											
ν_μ	Hyper-K E_ν^{QE}	1.0	2.2	0.6	0.9	0.0	0.1	0.0	0.3	0.5	0.8
	DUNE E_ν^{avail}	1.4	1.5	0.0	0.0	0.4	0.4	1.2	1.0	0.3	0.7
	DUNE E_ν^{had}	1.5	1.7	0.1	0.2	0.4	0.3	1.9	1.4	0.3	0.7
$\bar{\nu}_\mu$	Hyper-K E_ν^{QE}	0.5	1.5	0.3	0.7	0.0	0.0	0.1	0.1		
	DUNE E_ν^{avail}	0.5	0.6	0.1	0.2	0.4	0.4	1.1	1.1		
	DUNE E_ν^{had}	0.9	0.9	0.3	0.3	0.4	0.5	1.6	1.5		

Table 3: The shift in the mean and median neutrino energy estimation bias due to different FSI variations for the Hyper-K and DUNE neutrino and antineutrino cases. The top half reports the absolute shift in MeV, and the bottom half the same shift expressed as a fraction of E_ν^{true} (in percent). The numbers reported for the INC model variation are derived from the two INC models that give the largest spread in the mean. Red boxes indicate that the variation is larger than 5 MeV / 15 MeV (absolute, Hyper-K and DUNE respectively) or 0.5% (relative), which is broadly indicative of how well the neutrino energy reconstruction scale must be controlled (see [section 3](#)). “Nuc. Pot.” stands for the nuclear potential considered in [subsection 4.3](#), for which the table reports a shift derived considering only CCQE interactions.

References

- [1] Babak Abi et al. Deep Underground Neutrino Experiment (DUNE), Far Detector Technical Design Report, Volume II: DUNE Physics. 2 2020.
- [2] B. Abi et al. Long-baseline neutrino oscillation physics potential of the dune experiment. *Eur. Phys. J.*, C80:978, 6 2020.
- [3] K. Abe et al. Hyper-Kamiokande Design Report. 5 2018.
- [4] K. Abe et al. Sensitivity of the Hyper-Kamiokande experiment to neutrino oscillation parameters using acceleration neutrinos. 5 2025.
- [5] K. Abe et al. The T2K Experiment. *Nucl. Instrum. Meth. A*, 659:106–135, 2011.

- [6] D. S. Ayres et al. The NOvA Technical Design Report. *FERMILAB-DESIGN-2007-01*, 10 2007.
- [7] Ziro Maki, Masami Nakagawa, and Shoichi Sakata. Remarks on the Unified Model of Elementary Particles. *Progress of Theoretical Physics*, 28(5):870–880, 11 1962.
- [8] Samoil M. Bilenky and B. Pontecorvo. Lepton Mixing and Neutrino Oscillations. *Phys. Rept.*, 41:225–261, 1978.
- [9] S. Navas et al. Review of particle physics. *Phys. Rev. D*, 110(3):030001, 2024.
- [10] Jorge de Blas et al. Physics Briefing Book: Input for the 2026 update of the European Strategy for Particle Physics. 11 2025.
- [11] Yinrui Liu, Laura Munteanu, and Stephen Dolan. The role of final-state interaction modeling in neutrino energy reconstruction and oscillation measurements. 11 2025.
- [12] Artur M. Ankowski, Omar Benhar, and Makoto Sakuda. Improving the accuracy of neutrino energy reconstruction in charged-current quasielastic scattering off nuclear targets. *Phys. Rev. D*, 91(3):033005, 2015.
- [13] Artur M. Ankowski, Pilar Coloma, Patrick Huber, Camillo Mariani, and Erica Vagnoni. Missing energy and the measurement of the CP-violating phase in neutrino oscillations. *Phys. Rev. D*, 92(9):091301, 2015.
- [14] Alexander Friedland and Shirley Weishi Li. Understanding the energy resolution of liquid argon neutrino detectors. *Phys. Rev. D*, 99(3):036009, 2019.
- [15] Srishti Nagu, Jaydip Singh, Jyotsna Singh, and R. B. Singh. Impact of Cross-Sectional Uncertainties on DUNE Sensitivity due to Nuclear Effects. *Nucl. Phys. B*, 951:114888, 2020.
- [16] Adam Abed Abud et al. Deep Underground Neutrino Experiment (DUNE) Near Detector Conceptual Design Report. *Instruments*, 5(4):31, 2021.
- [17] Nina M. Coyle, Shirley Weishi Li, and Pedro A. N. Machado. Neutrino-nucleus cross section impacts on neutrino oscillation measurements. *Phys. Rev. D*, 111(9):093010, 2025.
- [18] Tomasz Golan, Cezary Juszczak, and Jan T. Sobczyk. Final State Interactions Effects in Neutrino-Nucleus Interactions. *Phys. Rev. C*, 86:015505, 2012.
- [19] T. Golan, Jan Sobczyk, and J. Żmuda. Nuwro: the wrocław monte carlo generator of neutrino interactions. *Nuclear Physics B Proceedings Supplements*, 229-232:499–499, 08 2012.
- [20] Hemant Prasad, Jan T. Sobczyk, Rwik Dharmapal Banerjee, J. Luis Bonilla, Krzysztof M. Graczyk, Beata E. Kowal, and Artur M. Ankowski. Fine-tuning final state interactions model in nuwro monte carlo event generator, 2025.
- [21] C. Andreopoulos et al. The GENIE Neutrino Monte Carlo Generator. *Nucl. Instrum. Meth. A*, 614:87–104, 2010.
- [22] Costas Andreopoulos, Christopher Barry, Steve Dytman, Hugh Gallagher, Tomasz Golan, Robert Hatcher, Gabriel Perdue, and Julia Yarba. The GENIE Neutrino Monte Carlo Generator: Physics and User Manual. 10 2015.
- [23] Y. Hayato. NEUT. *Nucl. Phys. Proc. Suppl.*, 112:171–176, 2002.
- [24] Yoshinari Hayato. A neutrino interaction simulation program library NEUT. *Acta Phys. Polon. B*, 40:2477–2489, 2009.
- [25] Yoshinari Hayato and Luke Pickering. The NEUT neutrino interaction simulation program library. *Eur. Phys. J. ST*, 230(24):4469–4481, 2021.
- [26] L. Alvarez-Ruso et al. NuSTEC White Paper: Status and challenges of neutrino–nucleus scattering. *Prog. Part. Nucl. Phys.*, 100:1–68, 2018.
- [27] J. A. Formaggio and G. P. Zeller. From eV to EeV: Neutrino Cross Sections Across Energy Scales. *Rev. Mod. Phys.*, 84:1307–1341, 2012.

- [28] A. Lozano et al. Measurement of charged-current ν_μ and $\bar{\nu}_\mu$ cross sections on hydrocarbon in a shallow inelastic scattering region. 3 2025.
- [29] Steven Dytman et al. Comparison of validation methods of simulations for final state interactions in hadron production experiments. *Phys. Rev. D*, 104(5):053006, 2021.
- [30] L. L. Salcedo, E. Oset, M. J. Vicente-Vacas, and C. Garcia-Recio. Computer Simulation of Inclusive Pion Nuclear Reactions. *Nucl. Phys. A*, 484:557–592, 1988.
- [31] D.H. Wright and M.H. Kelsey. The geant4 bertini cascade. *Nuclear Instruments and Methods in Physics Research Section A: Accelerators, Spectrometers, Detectors and Associated Equipment*, 804:175 – 188, 2015.
- [32] J. McKean, R. González-Jiménez, M. Kabirnezhad, J. M. Udías, and Y. Uchida. Implementation of a relativistic distorted wave impulse approximation model into the NEUT event generator. 2 2025.
- [33] Raúl González-Jiménez, Alexis Nikolakopoulos, Natalie Jachowicz, and JM Udías. Nuclear effects in electron-nucleus and neutrino-nucleus scattering within a relativistic quantum mechanical framework. *Physical Review C*, 100(4):045501, 2019.
- [34] Davide Mancusi, Alain Boudard, Jaume Carbonell, Joseph Cugnon, Jean-Christophe David, and Sylvie Leray. Improving the description of proton-induced one-nucleon removal in intranuclear-cascade models. *Phys. Rev. C*, 91(3):034602, 2015.
- [35] Alain Boudard, Joseph Cugnon, Jean-Christophe David, Sylvie Leray, and Davide Mancusi. New potentialities of the Liège intranuclear cascade model for reactions induced by nucleons and light charged particles. *Phys. Rev. C*, 87(1):014606, 2013.
- [36] Aleksandra Kelic, M. Valentina Ricciardi, and Karl-Heinz Schmidt. ABLA07 - towards a complete description of the decay channels of a nuclear system from spontaneous fission to multifragmentation. In *Joint ICTP-IAEA Advanced Workshop on Model Codes for Spallation Reactions*, 6 2009.
- [37] O. Buss et al. Transport-theoretical Description of Nuclear Reactions. *Phys. Rept.*, 512:1–124, 2012.
- [38] Joshua Isaacson, William I. Jay, Alessandro Lovato, Pedro A. N. Machado, and Noemi Rocco. Introducing a novel event generator for electron-nucleus and neutrino-nucleus scattering. *Phys. Rev. D*, 107(3):033007, 2023.
- [39] Alexis Nikolakopoulos, Raúl González-Jiménez, Natalie Jachowicz, Kajetan Niewczas, Federico Sánchez, and José Manuel Udías. Benchmarking intranuclear cascade models for neutrino scattering with relativistic optical potentials. *Phys. Rev. C*, 105(5):054603, 2022.
- [40] https://home.fnal.gov/~ljf26/DUNEFluxes/OptimizedEngineeredNov2017_offaxis/. Accessed: 2019-08-07.
- [41] K. Abe et al. The t2k neutrino flux prediction. *Phys. Rev.*, D87:012001, 2013.
- [42] J. Coelho. Probosc. [Online; accessed 28 May 2026].
- [43] Particle Data Group. Review of Particle Physics (2025 update): Neutrino Masses, Mixing, and Oscillations. <https://pdg.lbl.gov/2025/web/viewer.html?file=../reviews/rpp2025-rev-neutrino-mixing.pdf>, 2025. Review last revised 1 December 2025; accessed 21 May 2026.
- [44] Ivan Esteban, M. C. Gonzalez-Garcia, Michele Maltoni, Ivan Martinez-Soler, João Paulo Pinheiro, and Thomas Schwetz. NuFit-6.0: updated global analysis of three-flavor neutrino oscillations. *JHEP*, 12:216, 2024.
- [45] P. Stowell et al. NUISANCE: a neutrino cross-section generator tuning and comparison framework. *JINST*, 12(01):P01016, 2017.
- [46] Omar Benhar, A Fabrocini, S Fantoni, and I Sick. Spectral function of finite nuclei and scattering of gev electrons. *Nuclear Physics A*, 579(3-4):493–517, 1994.

- [47] L. Jiang et al. Determination of the argon spectral function from $(e, e'p)$ data. *Phys. Rev. D*, 105:112002, Jun 2022.
- [48] Rwik Dharmapal Banerjee, Artur M. Ankowski, Krzysztof M. Graczyk, Beata E. Kowal, Hemant Prasad, and Jan T. Sobczyk. Jlab spectral functions of argon in nuwro and their implications for microboone. *Physical Review D*, 109(7), April 2024.
- [49] Artur M. Ankowski, Rwik Dharmapal Banerjee, Jan T. Sobczyk, José L. Bonilla, Krzysztof M. Graczyk, Beata E. Kowal, and Hemant Prasad. Spectral function approach in NuWro: modeling of multinucleon final states in quasielastic scattering. 8 2025.
- [50] J. E. Sobczyk, J. Nieves, and F. Sánchez. Exclusive-final-state hadron observables from neutrino-nucleus multinucleon knockout. *Phys. Rev. C*, 102:024601, Aug 2020.
- [51] Hemant Prasad, Jan T. Sobczyk, Artur M. Ankowski, J. Luis Bonilla, Rwik Dharmapal Banerjee, Krzysztof M. Graczyk, and Beata E. Kowal. New multinucleon knockout model in the nuwro monte carlo generator. *Phys. Rev. D*, 111:036032, Feb 2025.
- [52] Qiyu Yan, Kajetan Niewczas, Alexis Nikolakopoulos, Raúl González-Jiménez, Natalie Jachowicz, Xianguo Lu, Jan Sobczyk, and Yangheng Zheng. The Ghent Hybrid model in NuWro: a new neutrino single-pion production model in the GeV regime. *JHEP*, 12:141, 2024.
- [53] M. Glück, E. Reya, and A. Vogt. Dynamical parton distributions revisited. *Eur. Phys. J. C*, 5:461–470, 1998.
- [54] A. Bodek and U. K. Yang. Modeling deep inelastic cross-sections in the few GeV region. *Nucl. Phys. B Proc. Suppl.*, 112:70–76, 2002.
- [55] Torbjorn Sjostrand, Stephen Mrenna, and Peter Z. Skands. PYTHIA 6.4 Physics and Manual. *JHEP*, 05:026, 2006.
- [56] Clarence Wret. Practicum: analyzing generator output, April 2024.
- [57] Stephen Dolan, Luke Pickering, Pickering Stowell, Callum Wilkinson, and Clarence Wret. CP-violation or Nuclear Excitation: Reviewing the Role of Neutrino Interaction Model Uncertainties on Accelerator-Based Neutrino Oscillation Measurements. In Preparation.
- [58] Júlia Tena-Vidal et al. Neutrino-nucleon cross-section model tuning in GENIE v3. *Phys. Rev. D*, 104(7):072009, 2021.
- [59] J. Nieves, I. Ruiz Simo, and M. J. Vicente Vacas. Inclusive Charged-Current Neutrino-Nucleus Reactions. *Phys. Rev.*, C83:045501, 2011.
- [60] Richard Gran, J Nieves, F Sanchez, and MJ Vicente Vacas. Neutrino-nucleus quasi-elastic and 2p2h interactions up to 10 gev. *Physical Review D*, 88(11):113007, 2013.
- [61] Jackie Schwehr, Dan Cherdack, and Rik Gran. GENIE implementation of IFIC Valencia model for QE-like 2p2h neutrino-nucleus cross section. 1 2016.
- [62] Ch. Berger and L. M. Sehgal. Lepton mass effects in single pion production by neutrinos. *Phys. Rev. D*, 76:113004, 2007.
- [63] Ch. Berger and L. M. Sehgal. Erratum: Lepton mass effects in single pion production by neutrinos [phys. rev. d 76, 113004 (2007)]. *Phys. Rev. D*, 77:059901, Mar 2008.
- [64] Torbjorn Sjostrand. High-energy-physics event generation with pythia 5.7 and jetset 7.4. *Computer Physics Communications*, 82(1):74 – 89, 1994.
- [65] T. Yang, C. Andreopoulos, H. Gallagher, K. Hoffmann, and P. Kehayias. A Hadronization Model for Few-GeV Neutrino Interactions. *Eur. Phys. J. C*, 63:1–10, 2009.
- [66] Júlia Tena-Vidal et al. Hadronization model tuning in genie v3. *Phys. Rev. D*, 105(1):012009, 2022.
- [67] Aatos Heikkinen, Nikita Stepanov, and Johannes Peter Wellisch. Bertini intranuclear cascade implementation in GEANT4. *eConf*, C0303241:MOMT008, 2003.

- [68] Robert Hatcher. Non-physics aspects of the integration of incl++ and geant4 into genie fsi. https://genie-docdb.pp.rl.ac.uk/DocDB/0001/000174/001/inclxx_and_g4.pdf, November 2019. Accessed: 2026-02-17.
- [69] Anna Ershova, Sara Bolognesi, Alain Letourneau, J-C David, Stephen Dolan, Jason Hirtz, Kajetan Niewczas, Jan T Sobczyk, Adrien Blanchet, M Buizza Avanzini, et al. Study of final-state interactions of protons in neutrino-nucleus scattering with incl and nuwro cascade models. *Physical Review D*, 106(3):032009, 2022.
- [70] R. González-Jiménez, M. B. Barbaro, J. A. Caballero, T. W. Donnelly, N. Jachowicz, G. D. Megias, K. Niewczas, A. Nikolakopoulos, and J. M. Udías. Constraints in modeling the quasielastic response in inclusive lepton-nucleus scattering. *Physical Review C*, 101(1), January 2020.
- [71] R. González-Jiménez, M. B. Barbaro, J. A. Caballero, T. W. Donnelly, N. Jachowicz, G. D. Megias, K. Niewczas, A. Nikolakopoulos, J. W. Van Orden, and J. M. Udías. Neutrino energy reconstruction from semi-inclusive samples. *Phys. Rev. C*, 105:025502, Feb 2022.
- [72] R. González-Jiménez, M. B. Barbaro, J. A. Caballero, T. W. Donnelly, N. Jachowicz, G. D. Megias, K. Niewczas, A. Nikolakopoulos, and J. M. Udías. Constraints in modeling the quasielastic response in inclusive lepton-nucleus scattering. *Phys. Rev. C*, 101(1):015503, 2020.
- [73] K. Abe et al. Improved constraints on neutrino mixing from the T2K experiment with 3.13×10^{21} protons on target. *Phys. Rev. D*, 103(11):112008, 2021.
- [74] P. A. Rodrigues et al. Identification of nuclear effects in neutrino-carbon interactions at low three-momentum transfer. *Phys. Rev. Lett.*, 116:071802, 2016. [Addendum: *Phys.Rev.Lett.* 121, 209902 (2018)].
- [75] Callum Wilkinson, Stephen Dolan, Luke Pickering, and Clarence Wret. A substandard candle: the low- ν method at few-GeV neutrino energies. *Eur. Phys. J. C*, 82(9):808, 2022.
- [76] D. Dutta et al. A Study of the quasielastic (e,e-prime p) reaction on C-12, Fe-56 and Au-97. *Phys. Rev. C*, 68:064603, 2003.
- [77] E. S. Pinzon Guerra et al. Using world charged π^\pm -nucleus scattering data to constrain an intranuclear cascade model. *Phys. Rev. D*, 99(5):052007, 2019.
- [78] K. Abe et al. Measurements of neutrino oscillation parameters from the T2K experiment using 3.6×10^{21} protons on target. *Eur. Phys. J. C*, 83(9):782, 2023.
- [79] S. Dytman et al. Proton Transparency and Neutrino Physics: New Methods and Modeling. 8 2025.
- [80] Kajetan Niewczas and Jan T. Sobczyk. Nuclear Transparency in Monte Carlo Neutrino Event Generators. *Phys. Rev. C*, 100(1):015505, 2019.
- [81] Elena Gramellini et al. Measurement of the π -Ar total hadronic cross section at the LArIAT experiment. *Phys. Rev. D*, 106(5):052009, 2022.
- [82] Saeed Abbaslu et al. Measurement of Exclusive π^+ -argon Interactions Using ProtoDUNE-SP. 11 2025.
- [83] Saeed Abbaslu et al. First Measurement of π^+ -Ar and p -Ar Total Inelastic Cross Sections in the Sub-GeV Energy Regime with ProtoDUNE-SP Data. 11 2025.
- [84] S. Bhadra et al. Letter of Intent to Construct a nuPRISM Detector in the J-PARC Neutrino Beamline. 12 2014.
- [85] K. Abe et al. The Hyper-Kamiokande experiment: input to the update of the European Strategy for Particle Physics. 6 2025.
- [86] T. Dieminger, S. Dolan, D. Sgalaberna, A. Nikolakopoulos, T. Dealtry, S. Bolognesi, L. Pickering, and A. Rubbia. Uncertainties on the ν_μ/ν_e , $\bar{\nu}_\mu/\bar{\nu}_e$ and $\nu_e/\bar{\nu}_e$ cross-section ratio from the modelling of nuclear effects and their impact on neutrino oscillation experiments. *Phys. Rev. D*, 108:L031301, 2023.

- [87] Artur M. Ankowski. Effect of the charged-lepton's mass on the quasielastic neutrino cross sections. *Phys. Rev. C*, 96(3):035501, 2017.
- [88] Alexis Nikolakopoulos, Natalie Jachowicz, Nils Van Dessel, Kajetan Niewczas, Raúl González-Jiménez, José Manuel Udías, and Vishvas Pandey. Electron versus Muon Neutrino Induced Cross Sections in Charged Current Quasielastic Processes. *Phys. Rev. Lett.*, 123(5):052501, 2019.
- [89] M. Martini, M. Ericson, and G. Chanfray. Phase space of electron- and muon-neutrino and antineutrino scattering off nuclei. *Phys. Rev. C*, 110(2):025502, 2024.